

A Year Later: Solar, Heliospheric, and Magnetospheric Disturbances in November 2004

Yu. I. Yermolaev¹, L. M. Zelenyi¹, G. N. Zastenker¹, A. A. Petrukovich¹, M. Yu. Yermolaev¹, N. S. Nikolaeva¹, M. I. Panasyuk², S. N. Kuznetsov², I. N. Myagkova², E. A. Murav'eva², B. Yu. Yushkov², I. S. Veselovsky², A. V. Dmitriev^{2,15}, A. N. Zhukov^{2,16}, O. S. Yakovchouk², V. D. Kuznetsov³, I. M. Chertok³, V. N. Ishkov³, A. V. Belov³, E. A. Eroshenko³, V. G. Yanke³, S. P. Gaidash³, Kh. D. Kanonidi³, S. V. Kuzin⁴, I. A. Zhitnik⁴, A. P. Ignat'ev⁴, V. A. Slemzin⁴, N. K. Sukhodrev⁴, S. A. Shestov⁴, M. V. Eselevich⁵, V. G. Eselevich⁵, G. V. Rudenko⁵, V. M. Dvornikov⁵, V. E. Sdobnov⁵, M. V. Kravtsova⁵, V. M. Bogod⁶, V. S. Kotel'nikov⁶, L. A. Pershakov⁷, M. I. Beloglazov⁷, V. I. Vlasov⁸, I. V. Chashei⁸, N. G. Kleimenova⁹, O. V. Kozyreva⁹, V. I. Kozlov¹⁰, V. A. Parkhomov¹¹, Yu. A. Kugaenko¹², R. Z. Khisamov¹³, V. L. Yanchukovskii¹³, and K. Kudela¹⁴

¹ Space Research Institute, Russian Academy of Sciences (IKI RAN), Profsoyuznaya ul. 84/32, Moscow, 117997 Russia

² Skobel'syn Research Institute of Nuclear Physics, Moscow State University (NIIYaF MGU), Vorob'evy gory, Moscow, 119899 Russia

³ Pushkov Institute of Terrestrial Magnetism, Ionosphere, and Radiowave Propagation, Russian Academy of Sciences, Troitsk, Moscow oblast, 142190 Russia

⁴ Lebedev Physics Institute, Russian Academy of Sciences (FIAN), Leninskii pr. 53, Moscow, 119991 Russia

⁵ Institute of Solar–Terrestrial Physics (ISZF), Siberian Division, Russian Academy of Sciences, P.O. Box 4026, Irkutsk, 664033 Russia

⁶ Special Astronomical (Pulkovo) Observatory, Russian Academy of Sciences, Pulkovskoe sh. 65, St. Petersburg, 196140 Russia

⁷ Polar Geophysical Institute (PGI), Kola Scientific Center, Russian Academy of Sciences, ul. Fersmana 14, Apatity, Murmansk oblast, 184209 Russia

⁸ Pushchino Radio Astronomy Observatory, Lebedev Physics Institute, Russian Academy of Sciences, Pushchino, 142292 Russia

⁹ Schmidt Institute of Physics of the Earth, Russian Academy of Sciences, Bol'shaya Gruzinskaya ul. 10, Moscow, 123810 Russia

¹⁰ Shafer Institute of Cosmophysical Research and Aeronomy, Siberian Division, Russian Academy of Sciences, pr. Lenina 31, Yakutsk, 677007 Russia

¹¹ Baikal State University of Economics and Law, Irkutsk, Russia

¹² Kamchat Branch, Geophysical Service, Russian Academy of Sciences, Petropavlovsk-Kamchatskii, Russia

¹³ Cosmic Ray Station, Novosibirsk Geophysical Observatory, Geophysical Service, Siberian Division, Russian Academy of Sciences, Novosibirsk, Russia

¹⁴ Institute of Experimental Physics, Academy of Sciences of Slovakia, Košice, Slovakia

¹⁵ Space Science Institute, Taiwan

¹⁶ Belgian Royal Observatory, Brussels, Belgium

Received May 18, 2005; in final form, July 21, 2005

Abstract—A year after the extreme events on the Sun, in the heliosphere, and on the Earth in October–November 2003 [Veselovsky *et al.*, 2004; Panasyuk *et al.*, 2004; Yermolaev *et al.*, 2005], a similar situation was also observed in November 2004. The main data observed when the strongest magnetic storm with $Dst = -373$ nT occurred on the Earth are presented in the paper prepared mainly by the participants of the last year's collaboration of native researchers of extreme events. The disturbance of the Sun, solar wind, and magnetosphere during the considered period was weaker than during the similar period in 2003 with respect to a number of parameters; nevertheless, the presented data indicate that the decline phase of solar cycle 23 is one of the most active intervals over the entire period of comprehensive studies of the solar–terrestrial coupling owing to the events that occurred in autumn 2003 and 2004.

1. INTRODUCTION

Studying the effect of solar and interplanetary (heliospheric) events on the near-Earth space is still the most important component of the solar–terrestrial physics. Since such an effect, often called space weather, is important in many areas of human activity, the studies in this direction are developed rapidly. In spite of the fact that the general concept of such an effect has been almost constant for many years and the large body of experimental and theoretical data has been accumulated by the present (see, e.g., the collected volumes and reviews [Gonzalez *et al.*, 1999, 2004; Crooker, 2000; Richardson *et al.*, 2001; Bothmer *et al.*, 2002; Yermolaev and Yermolaev, 2003; Cole, 2003; Lyatsky and Tan, 2003; Daglis *et al.*, 2003; Maltsev, 2004; Echer and Gonzalez, 2004; Yermolaev *et al.*, 2005; Dmitriev *et al.*, 2005; Kane, 2005; Schwenn *et al.*, 2005] and references therein), it is to a certain degree difficult to predict effects of the space weather. In this case it is possible to very accurately predict the response of the magnetosphere and underlying Earth’s regions based on measurements of the interplanetary medium parameters near the Earth’s magnetosphere (specifically, at the libration point $L1$); however, the degree of validity of a similar prediction based on solar observations remains rather low [Yermolaev and Yermolaev, 2003; Kane, 2005; Schwenn *et al.*, 2005; Yermolaev *et al.*, 2005]. This is related to the facts that, on the one hand, the studied system is complicated and includes many independent links where different physical mechanisms operate and, on the other hand, the experimental data are limited and are obtained only at certain spatial points that can be reached by up-to-date instrumentation. Therefore, integrated interdisciplinary studies are most promising and are carried out in our country and abroad. An excellent example of such an approach can be a “brain assault” of

the collaboration of the native researchers from more than ten scientific institutions, which was organized by IKI RAN and NIIYaF MGU in order to study the extreme events that occurred on the Sun, in the heliosphere, and on the Earth in October–November 2003. Extensive data on these events were collected over a relatively short time interval; the “International Symposium on Solar Extreme Events of 2003: Fundamental Science and Applied Aspects” was held in Moscow on July 12–14, 2004; and several reviews [Veselovsky *et al.*, 2004; Panasyuk *et al.*, 2004; Yermolaev *et al.*, 2005] and specific papers (see *Cosmic Research*, no. 6, 2004 and *Geomagnetism and Aeronomy*, no. 1, 2005) were published. Together with the foreign studies of these events (see the papers in the special issue of the journal *Geophysical Research Letters*, Vol. 32, no. 12, 2005 and references therein), these results made it possible to substantially progress in understanding the regularities of the solar–terrestrial physics using the extreme events of October–November 2003 as an example.

Exactly a year later, at the end of October–beginning of November 2004, the Sun was again very active and generated a number of strong interplanetary and magnetospheric disturbances (Fig. 1, Table 1). The values of some parameters measured during this period of 2004 were slightly smaller than the extreme values observed in 2003 (three X-class solar flares as compared to 11 such flares in 2003 and the magnetic storm with $Dst = -373$ nT as compared to the storm with $Dst = -401$ nT in 2003); nevertheless, solar activity in 2004 can be considered among the strongest events not only in the current solar activity cycle (cycle 23) but also during the entire period of space observations. The group of researchers, which was mainly formed during an analysis of the previous active period, collected and analyzed new data on the Sun and heliosphere before the magnetic storm of November 8–10, 2004, and on

Table 1. Flare events in AR 10696 in November 2004 and their manifestations in the near-Earth space

Ord. no.	Date, UT, duration (min)	Coordinates	Class	CME	ISW date/UT	Magnetic storm date Dst
1	Nov. 3, 1535, 59	N11 E40	M5.0/SN	NE		
2	Nov. 4, 0845, >79	N08 E28	C6.3/SN	P.Halo	7/0200	
3	Nov. 4, 2142, >131	N11 E19	M2.5/1N	P.Halo		
	Nov. 4, 2234		M5.4/1N	P.Halo	7/1000	
4	Nov. 5, 1123, >10	N08 E15	M4.0/1F	–		
	Nov. 5, 1910	N09 E07	M1.2/SF	–		
5	Nov. 6, 0011, 157	N10 E08	M9.3/2N	Halo		
	Nov. 6, 0044		M5.9	Halo	7/1755	
	Nov. 6, 0140		M3.6	Halo		Nov. 8 –373 nT
6	Nov. 7, 1542, >33	N09 W17	X2.0/2B	Halo	9/1818	
7	Nov. 9, 1659, 90	N07 W51	M8.9/2N	Halo		
8	Nov. 10, 0159, 76	N09 W49	X2.5/3B	Halo		Nov. 10 –289 nT

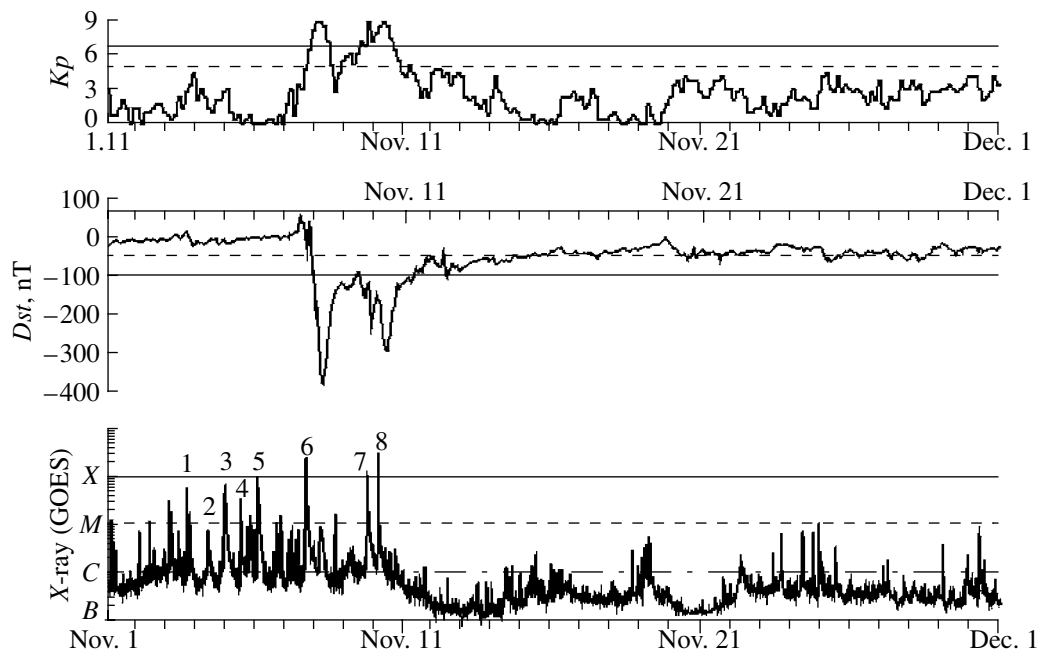


Fig. 1. The series of solar and ground-based measurements in November 2004. The upper and middle panels: the Kp and Dst indices (dashed and solid lines are the boundaries of moderate and strong magnetic storms). The Lower panel: the X-ray emission according to the GOES-12 satellite measurements (letters X, M, B, and C on the axis and different lines show flare classes). Nos. 1–8 correspond to the flares presented in Table 1.

the state of the Earth's magnetosphere at that time presented in this work. This work is preliminary, and its aim is to generally describe the state of different spatial regions during that period and to present the main Russian and foreign experimental data that can be used in a further analysis.

2. SOLAR OBSERVATIONS

2.1. General Description of Solar Events

The burst of solar-flare and eruptive activity at the decline phase of the current solar cycle (cycle 23) was observed at the end of October–beginning of November 2004. This burst was related to the passage of two sunspot groups–active regions (ARs) 10691 and 10696–over the visible solar disk. One X-class flare and seven M-class flares occurred in AR 10691 during 38 h from October 30 to November 1. The consequences of this activity in the near-Earth space were rather weak: two proton events of low intensity and a number of sudden ionospheric disturbances of a medium power; however, geomagnetic disturbances were not observed. This was apparently related to the position of the active region relative to the Sun–Earth line since the AR heliolongitude changed from W20 to W60 during this period and potentially effective disturbances could pass over the Earth. Therefore, it is more interesting to analyze the effect of the Sun on the Earth using solar activity in another active region (AR 10696).

Considered activity was related to a rapid development of AR 10696 (coordinates N09, Carrington longitude $L = 026$) (Fig. 2). According to the data presented in the Preliminary Report and Forecast of Solar Geophysical Data (see <http://www.sel.noaa.gov/weekly/pdf/prf1523> and [1524.pdf](http://www.sel.noaa.gov/weekly/pdf/prf1524)), from November 1 (heliolongitude E63) to November 6 (W08), the sunspot area in this region increased from 60 to 910 millionth parts of hemisphere (m.p.h.), the number of sunspots in this region increased from 6 to 33, and the magnetic configuration changed from simple (β) to flare-productive ($\beta\gamma\delta$). The number and area of sunspots began to decrease after November 6 and repeatedly increased to 48 on November 8 and to 730 m.p.h. on November 9, respectively. A rapid evolution of AR 10696 was accompanied by high sunspot activity: 13 M- and two X-class X-ray flares occurred when the active region crossed the disk (Fig. 1).

High flare activity was combined with very high eruptive activity. During November 3–10, the SOHO/LASCO white light coronagraph registered many considerable coronal mass ejections (CMEs) including nine CMEs of a halo type with a emission around significant part or the entire occulting disk of the coronagraph. Figure 3 presents the difference images of these CMEs. For each event, these images were obtained using the LASCO/C3 coronagraph data by subtracting a background image before eruption from images at the phase of development of the corresponding CME. The CME shape in the plane of the pic-

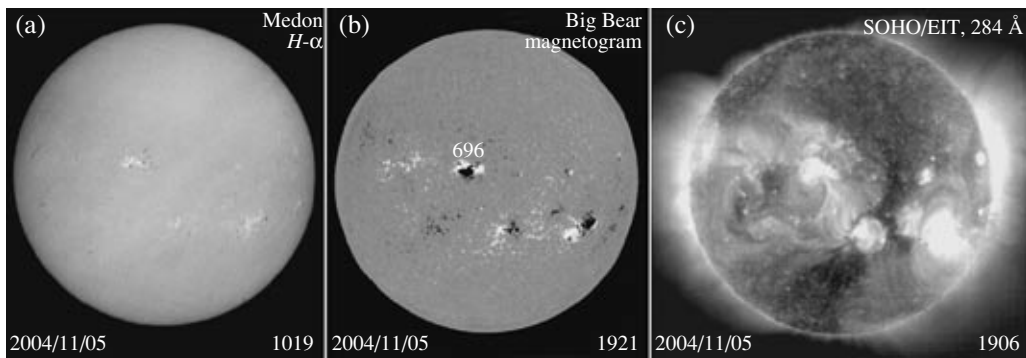


Fig. 2. Heliograms in the (a) H_{α} line and (c) 284 Å UV channel for November 5, 2004. (b) The fields of the northern and southern polarities are light and dark, respectively. AR 10696—the main source of flare activity—is localized.

ture indicates that these ejections are large-scale and even global: the CME linear dimensions were several ten times as large as the visible disk diameter even at distances of 10–20 R_{\odot} (solar radii) from the Sun. In this case the brightest CME structures shifted from the northeastern to the northern and then to the northwestern sectors of the near-Sun space as AR 10696 crossed the disk. Emission observed around other limb sectors indicates that the CME angular dimensions were considerable and the component of CME propagation in the direction perpendicular to the plane of the picture, in this case toward the Earth, could be substantial.

The chronological development of the flare and eruptive events in the considered sunspot group was as follows: the first M1.6/1N flare event was registered near noon on November 3 (the emission maximum was observed at 1335 UT) and was accompanied by dynamic radio bursts of types II and IV and by a bright CME directed northeastward. A large M5.0/SN flare event occurred at 1535 UT and was accompanied by radio bursts of types II and IV and by a considerable asymmetric CME (appeared for the first time at 1606 UT according to the data of the C3 coronagraph on SOHO), which developed on the northeastern limb with a sky-plane speed of about 900 km/s. An M1.0/SF flare, which occurred at 1803 UT and was also accompanied by an asymmetric CME of low intensity, was the last event of this day. A long-duration C6.3/SF flare event occurred 14 h later (at 0845 UT on November 4) and was accompanied by a significant radio burst of type IV and by a rather large partial halo CME (at 1042 UT) with the main ejection developed northeastward at a sky-plane speed of ~ 635 km s $^{-1}$. A rather rare event occurred at the end of November 4: two M2.5 (at 2142 UT) and M5.4 (at 2253 UT) X-ray flares with radio bursts of types II and IV were observed during a 1N optical flare that continued for more than 2 h. The initial phase of this flare, corresponding to the first X-ray flare, occurred in the following part of the sunspot group. When the second X-ray flare began, the emission occupied the group center and one emission ribbon reached

the penumbra of the leading sunspot. This flare event generated a complicated partial halo CME (at 2342 UT) with propagation of two disturbance fronts [LASCO CME List 2004, ftp://lasco6.nascom.gov/pub/lasco/status/LASCO_CME_List_2004]. The first front developed mainly near the northeastern (NE) limb, whereas the second front occupied the western hemisphere (covered about 290° according to the C3 data). The mean sky-plane speed of CME propagation was ~ 1050 km s $^{-1}$. November 5 was a relatively quiet day since both M4.0/1F (1123 UT) and M1.2/SF (1910 UT) flares were not accompanied by CMEs.

Flares and CME that occurred on November 3–5, when AR 10696 was located on the eastern hemisphere, did not result in considerable disturbances in the near-Earth space. Energetic particles, which were possibly accelerated during these events, apparently passed east and northeast of the Earth propagating along the helical IMF lines. Disturbances of the interplanetary medium and the magnetosphere caused by these solar events are considered in detail in the next sections of this paper (see Figs. 11, 12, Table 4).

At the beginning of November 6, a rather rare flare event occurred in the active region located near the central meridian (N09 E05). A 2N optical flare “combined” three considerable X-ray flares: M9.3 (0011 UT) with dynamic radio bursts of types II and IV, M5.9 (0044 UT), and M1.4 (0140 UT). However, this activity (as well as the events of November 3–5) did not lead to an increase in the near-Earth flux of energetic protons. This flare event resulted in a complicated full halo CME with three clearly defined components started at 0131, 0206, and 0242 UT (according to the C3 data, Fig. 3). The mean speed of disturbance propagation in the sky-plane was about 960 km s $^{-1}$. The strongest geomagnetic storm with a *Dst* minimum of about -373 nT at 0700 UT on November 8 (Fig. 1) was preceded by three pulses of sudden commencement (SC) registered at 0257, 1052, and 1827 UT on November 7, respectively. This indicates that the corresponding interplanetary disturbance was complicated and the preceding

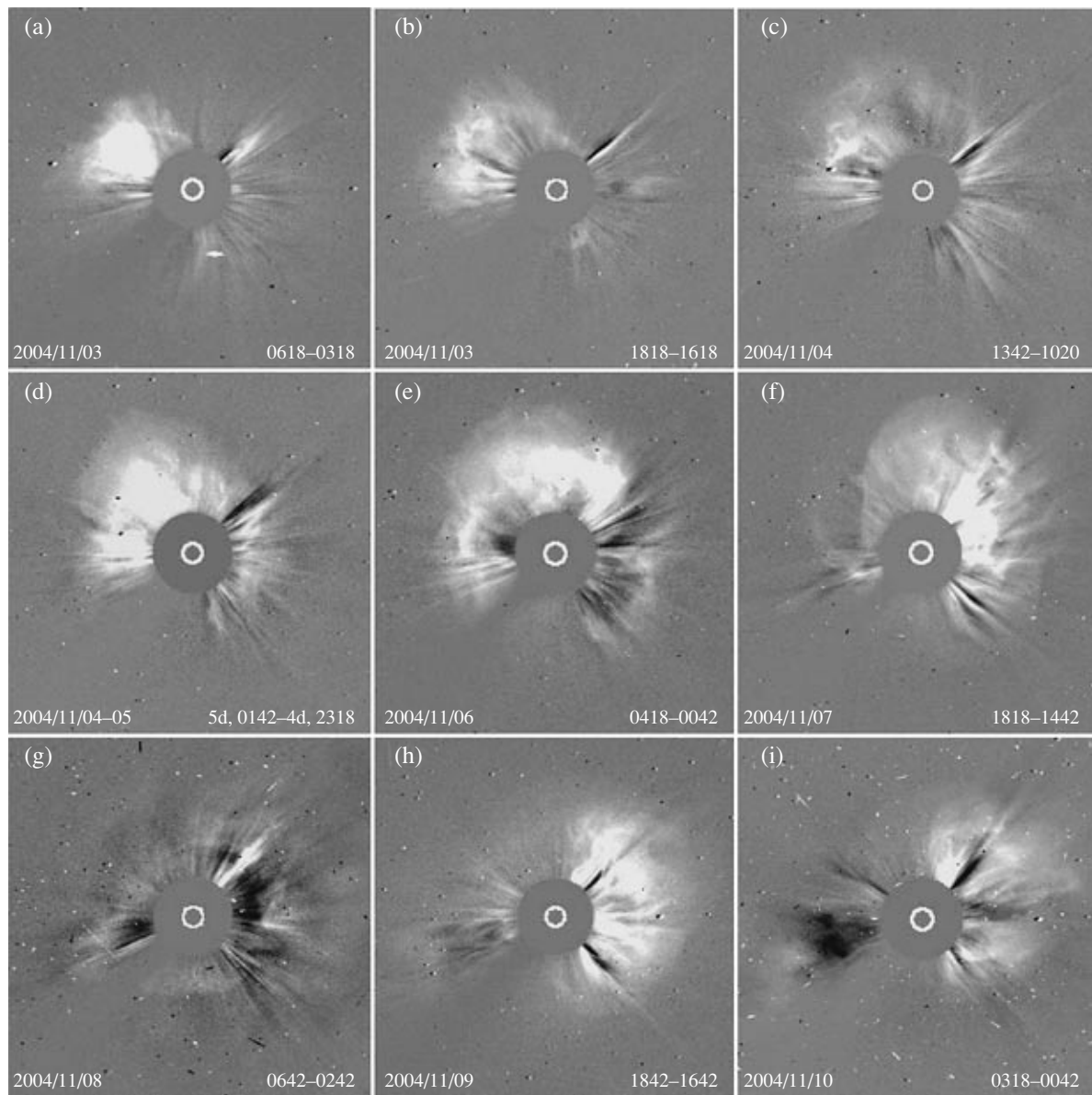


Fig. 3. Difference images of the largest “halo” CMEs registered by the SOHO/LASCO/C3 white light coronagraph on November 3–10, 2004. Dates and times of the main and background frames are shown at the bottom of each frame.

eruptive events that occurred on the Sun in the middle of November 4 (Fig. 3c), on the night of November 4–5 (Fig. 3d), and during November 5 (Fig. 2) possibly contributed to this disturbance (see Table 4).

Finally, on November 7 the active region generated the X2.0/2B flare (1542 UT) which was the strongest event during the first period of flare energy release. This flare was accompanied by the most intense radio signal at all observed frequencies, dynamic radio bursts of types II and IV, and full halo CMEs. According to the C3 SOHO data, the bright and very wide loop front developed mainly to WNW and slightly moved southward forming full halo (see <ftp://lasco6.nascom.gov/>

pub/lasco/status/LASCO_CME_List_2004). The ejection first appearance in C3 was registered at 1718 UT. The mean sky-plane speed of disturbance propagation was 1460 km/s. Since AR 10696 was located at that time on the western hemisphere (coordinates N09W17), this event was accompanied by a considerable increase in the near-Earth proton flux, the maximum of which at energies $E > 10$ MeV reached $4.6 \times 10^2 \text{ cm}^{-2} \text{ s}^{-1} \text{ sr}^{-1}$ (Fig. 11). SC registered at 0930 UT on November 9, which corresponds to an interplanetary shock estimated velocity of about 1000 km/s, is probably related to this event. The second eruptive event, which could contribute to the geomagnetic storm of

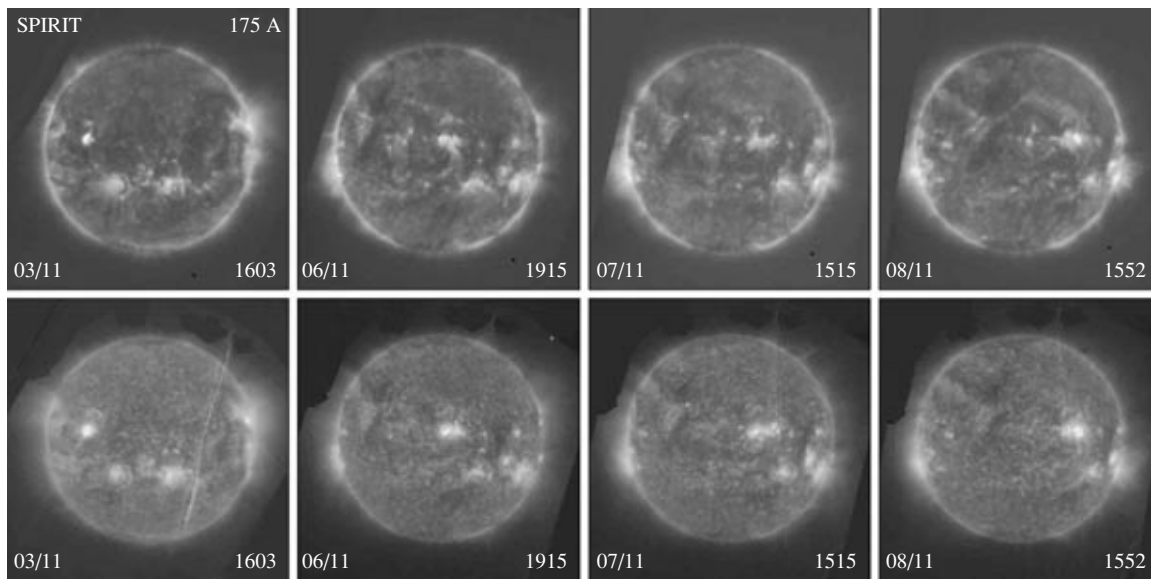


Fig. 4. SPiRiT/CORONAS-F images of the Sun in the 175 and 304 Å channels obtained on November 3–8, 2004.

November 10 with $Dst \approx -289$ nT, was observed at 0330 UT on November 8 as a less intense (SF/C7.9; coordinates N08W28) but more prolonged flare (Fig. 1) and a relatively faint diffuse and slow ($V \approx 430$ – 520 km s $^{-1}$) full halo CME (Fig. 3g). At 1543 UT on November 8, this active region generated the next M2.3/1N flare with a very feeble CME registered at 1730 UT.

The second period of flare activity, which was maintained by the new outflow in driven and central parts of the sunspot group on November 6–7, began on November 9. Two large flares (2N/M8.9 flare, coordinates N07W51, at 1719 UT on November 9 and 3N/X2.5 flare, coordinates N09W49, at 0213 UT on November 10) and two CMEs (full halo CME at 1748 UT on November 9 with a sky-plane speed of 1800 km s $^{-1}$ and “asymmetric full halo” CME at 0242 UT on November 10 with a mean sky-plane speed

of disturbance propagation of about 2000 km s $^{-1}$) occurred in the active region over 9 h when a bright emission was observed over the entire western limb (Figs. 1, 3h, 3i). Since the sources were localized in the western disk sector, these events did not result in substantial geomagnetic disturbances but were accompanied by one more growth of the proton flux with a peak intensity of $(3\text{--}4) \times 10^2$ cm $^{-2}$ s $^{-1}$ sr $^{-1}$ (Fig. 11).

We should also state that the magnetic polarity distribution in AR 10696 was a substantial factor responsible for the intensity of the geomagnetic storms of November 8 and 10. The magnetogram in Fig. 2b indicates that positive and negative polarities dominated in the northern and southern zones of the region, respectively. If we assume, following Pudovkin *et al.* [1977], that during eruption the magnetic field is somehow carried by an interplanetary disturbance and the field polarity remains unchanged in the source, the above

Table 2. Flares and CMEs registered by the SPiRiT telescope on November 1–9, 2004

Date	Flare class	Flare beginning-max-end (GOES)	AR no.	CME beginning (UT)*	Direction*	CME angle width*	V, km s $^{-1}$ (linear approx.)*
Nov. 3, 2004	M5.0	1535-1547-1555	696	1606	342	316(H)	781
Nov. 6, 2004	M3.6	0140-0157-0208	696	0131	036	196	612
				1554	120	20	1953
Nov. 7, 2004	X2.0	1542-1606-1615	696	1554(?)			
Nov. 8, 2004	M2.3	1543-1549-1552	696	1430	313	26	558
				1630	325	10	220

* LASCO/SOHO data processed using the CACTUS program developed at Belgian Royal Observatory (see <http://sidc.oma.be/cactus/out/latestCMEs.html>).

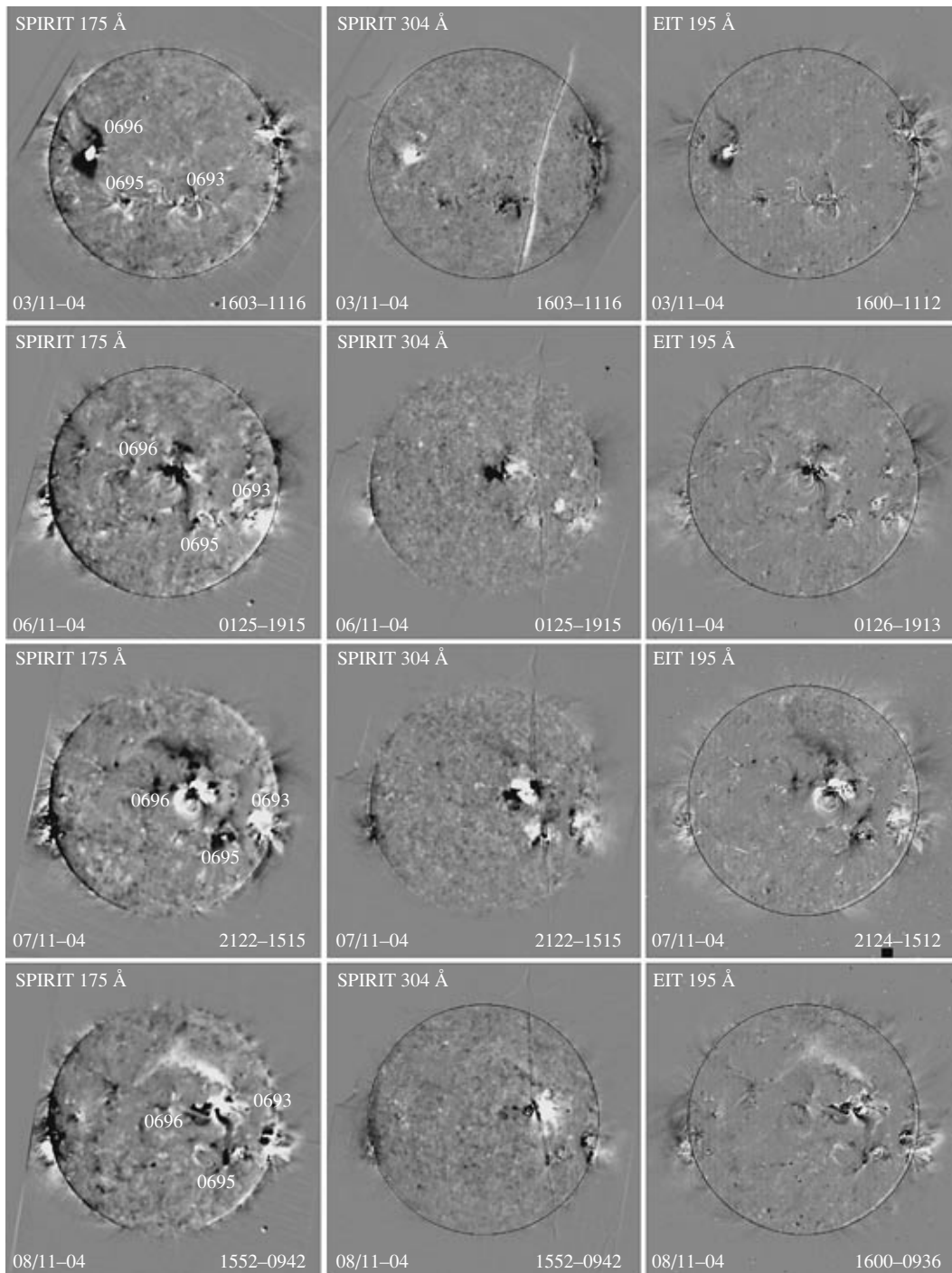


Fig. 5. Fixed difference images in the 175 and 304 Å channels of the SPIRIT telescope and similar images in the 195 Å channel of the SOHO/EIT telescope obtained on November 3, 6, 7, and 8, 2004. The times of registration of the current and base images are shown in the lower right-hand corner.

polarity distribution on the Sun had to result in a substantial negative B_z component near the Earth, precisely which was observed during the geomagnetic storms of November 8 and 10 (see subsection 3.1, Fig. 12).

The described eruptive events (specifically, large CME of November 6–10 and corresponding interplanetary disturbances) resulted also in a complicated, deep, and prolonged Forbush decrease in the GCR

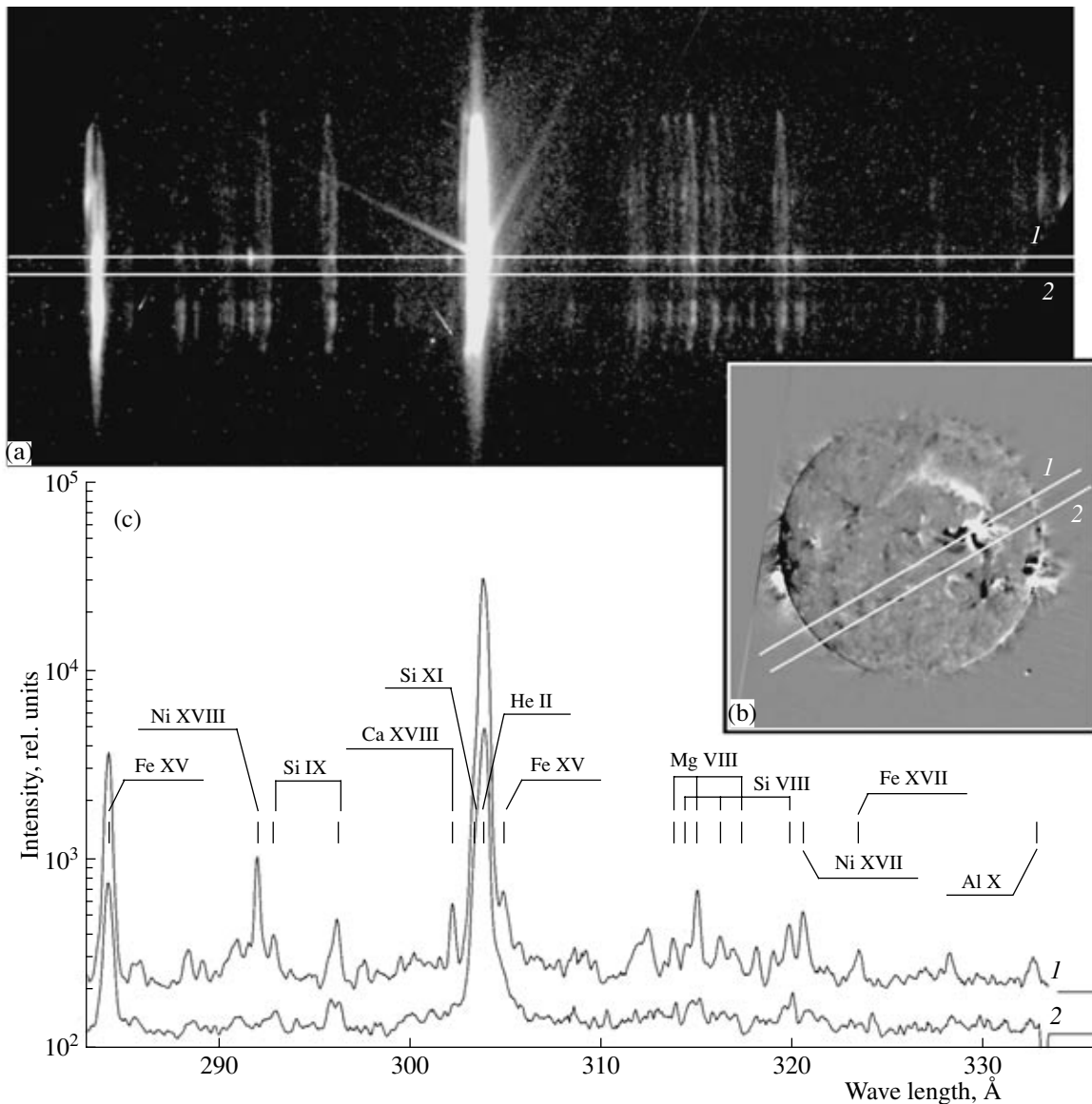


Fig. 6. (a) Spectrogram of the Sun in the 285–335 Å spectral region obtained during the flare of November 8, 2004 (1549:28 UT); (b) dispersion directions and scans on the solar disk; and (c) spectra along scans 1 (flare region) and 2 (dimming region and quiet areas).

intensity. This decrease started on November 7 simultaneously with the first geomagnetic storm and reached the maximal amplitude on November 10, and the recovery phase of this event lasted up to the middle of November (for details see subsection 3.4, Table 5).

2.2. Solar Activity Dynamics according to CORONAS-F/SPIRIT Data

The SPIRIT telescope on the CORONAS-F satellite was used in the observations performed on November 1–8, 2004 [Oraevskii *et al.*, 2002]. In this case the full disk images in the channels 175 and 304 Å were registered four times a day at intervals of 4–8 h and complete spectrograms were registered two times a day. Several

obtained telescopic images are shown in Fig. 4. Table 2 presents the times of flares and CMEs occurred during this period, for which SPIRIT data are available.

2.2.1. Dimmings. Fixed difference images, which reflect total activity changes between two successive frames, were constructed in order to study the structures of dimmings (local variations in the emission intensity on the solar disk). Images corresponding to instants before flares were selected as reference pictures. The next images in both channels were turned against solar rotation to the time of base frames, and base images were subsequently subtracted from these images. Brightness in difference images was reduced to the nonlinear scale in order to make dimmings more contrasting.

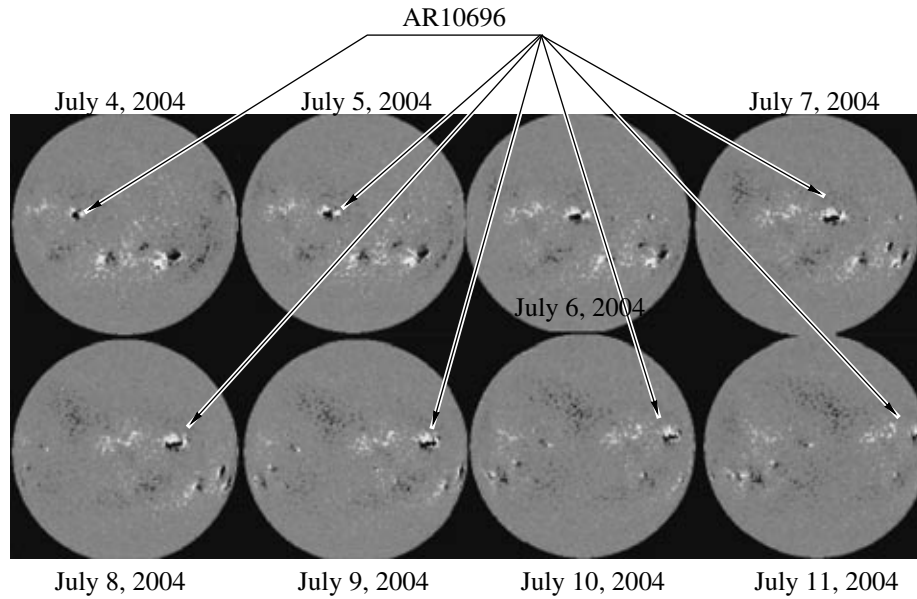


Fig. 7. SOHO MDI solar disk magnetograms. The magnetic structure of AR 10696 monotonically varies during the entire period.

Fixed difference images obtained using the SPIRIT telescope and similar SOHO/EIT images are compared in Fig. 5. All events listed in Table 2 occurred in a large complex which combines ARs 10693, 10695, and 10696.

A classical pair of compact dimmings, corresponding to footpoints of an eruptive magnetic loop, was generated as a result of the flare and eruptive event occurred on November 3 near AR 10696. These dimmings are very contrasting in the channels 175 and 195 Å and are much less distinct in the channel 304 Å, which can be caused by the delay in the dimming development in the transition layer [Chertok *et al.*, 2004].

Several dimmings were registered on November 6. A contrasting compact dimming east of AR 10696 and a narrow northwestward dimming were observed in all channels. An extensive southwestward dimming toward AR 10695 was also observed in the coronal channels 175 and 195 Å. This dimming is not observed in the transition layer channel 304 Å and possibly replaced a high transequatorial loop with a temperature of about 1–2 MK that existed previously and is invisible in the channel 304 Å.

Eruptive events of November 7 resulted in the generation of several large-scale dimmings near ARs 10696, 10695, and 10693, which indicates that the magnetic structures of these regions are closely interrelated. In addition to compact dimmings near ARs 10696, 10695, and 10693, a diffuse extensive dimming was formed north of AR 10696 in place of brightening previously observed in the initial images at the boundary of a low-latitude coronal hole.

On November 8, the dimming pattern was generally the same as on the preceding day; however, an exten-

sive dimming similar to a dimming of November 6 appeared in coronal lines between ARs 10696 and 10695 in addition to compact dimmings near all three ARs. This indicates that a transequatorial loop of the scale $R/2 \sim 300\,000$ km recovered during two days. In addition to dimmings, the difference images also indicate that brightness recovered in the region of a diffuse dimming to the north of AR 10696 and a high arc system appeared near AR 10693 stretching outside the limb; however, the relation of these events to flares and CMEs that occurred during this period is not evident.

Chertok [2005] analyzed in detail large-scale solar activity related to the considered series of flares and CMEs using the SOHO/EIT UV telescope data

Table 3. Ion spectral lines observed during the flare of November 8, 2003

Ion	Wavelength, Å	$\log_{10}(T_{\max})$
He II	303.78	4.9
Si VIII	314.36, 316.22, 319.84	5.9
Mg VIII	313.74, 315.02, 317.03	6.0
Al X	332.79	6.1
Si IX	292.81, 296.16	6.1
Si XI	303.33	6.2
Fe XV	284.16	6.4
Ni XVIII	291.98	6.7
Fe XVII	323.47	6.9
Ca XVIII	302.19	7.0

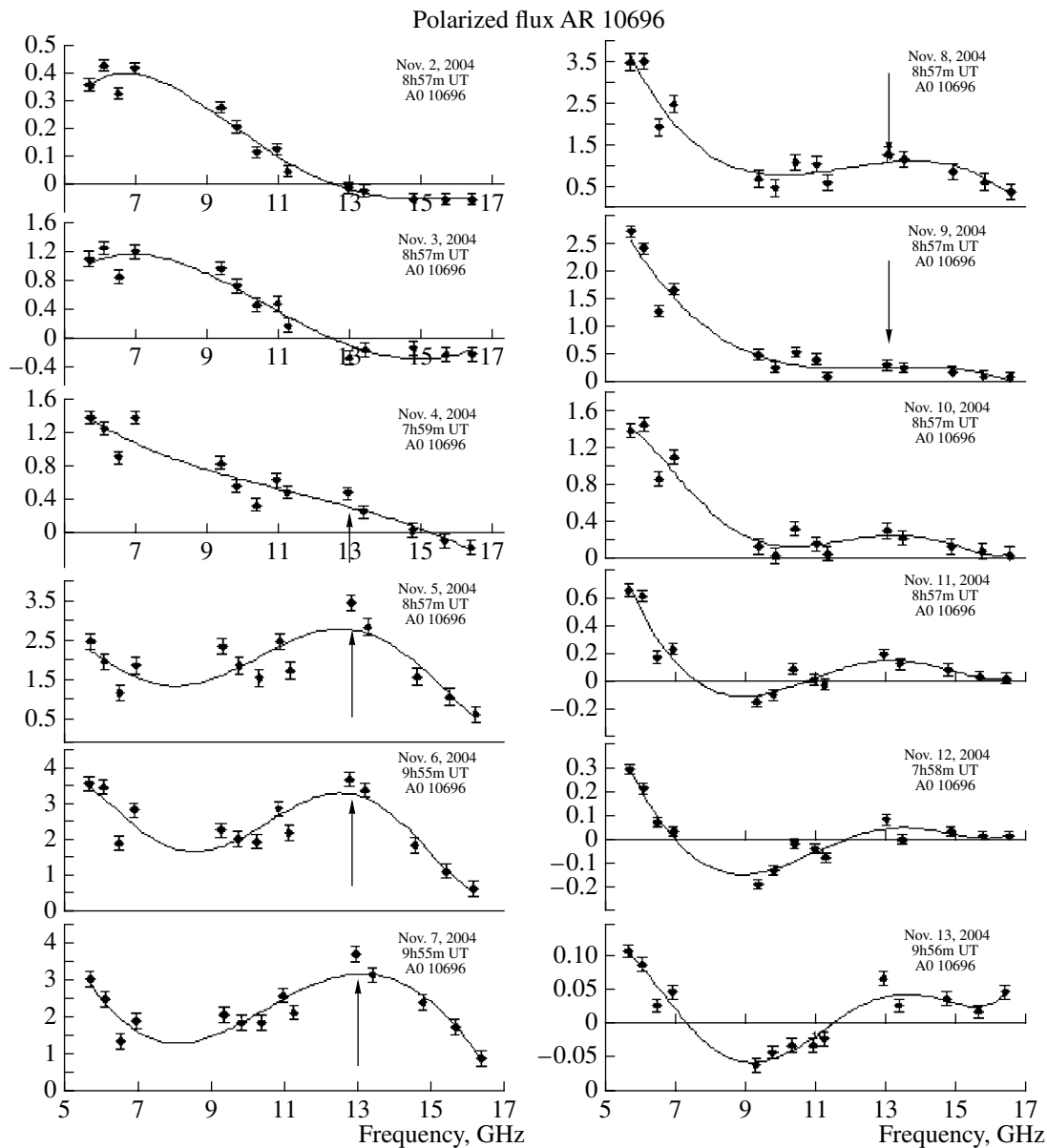


Fig. 8. The dynamics of the total polarized emission flux spectrum of AR 10696 from November 2 to November 11 according to the RATAN-600 data. The spectrum growth at high frequencies (11–16 GHz) is pronounced on November 4–7 (shown by the upward arrow). The emission flux sharply decreases on November 8 and 9 (downward arrow) due to the effect of darkening (see also Fig. 10).

(see also different heliograms and movies at the Web site http://helios.izmiran.troitsk.ru/lars/Chertok/04_11/index.html).

2.2.2. November 8, 2004, flare spectrum in the band 285–335 Å. Figure 6 demonstrates the SPIRIT spectrogram of the Sun in the 285–335 Å spectral region obtained at 1549:28 UT at an exposure of 150 s, i.e., almost at X-ray flare maximum according to the GOES data. In individual spectral lines, the Sun images have the shape of ellipsoids oblate in the dispersion direction [Beigman *et al.*, 2005]. The linear scan of the spectrogram in the direction of dispersion shows the

convolution of the spectral lines with brightness distributed along the given disk section. Scan 1 on the spectrogram crosses the flare region, and scan 2 is shifted (for comparison) so that it crosses the dimming region and quiet sectors of the disk. The orientation of the scans relative to the disk is shown in Fig. 6b, and the obtained spectra are demonstrated and deciphered in Fig. 6c. The brightest ion lines distinguished in the spectra are presented in Table 3 [Beigman *et al.*, 2005].

Hot lines of the flare region with the excitation temperature $\log_{10}(T) > 6.4$ (Ca XVIII, Ni XVIII, Fe XVII), which are almost absent in spectrum 2, are

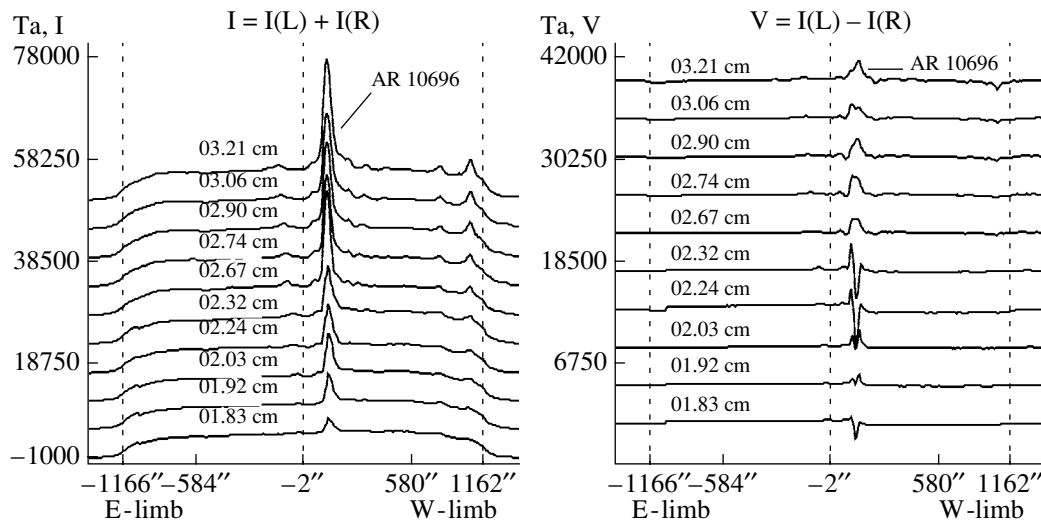


Fig. 9. Intensity (on the left) and circular polarization (on the right) radioemission scans at 0758 UT on November 7, 2004, according to the RATAN-600 data. Sharp changes and inversions are observed in the circular polarization channels.

clearly defined in spectrum 1 obtained in scan 1. The remaining lines with the excitation temperature $\log_{10}(T) = 5.9\text{--}6.2$ are observed in both spectra; however, their maximal brightness in the flare region is higher than brightness in the quiet regions by a factor of approximately 2–3. Thus, we can state that the temperature in the flare region was not lower than 10 MK when the spectrogram was obtained, and the emission measure in the region of temperatures 0.8–1.5 MK was two–three times as high as in the surrounding regions. The technique for determining the differential emission measure based on the data of the SPIRIT XUV spectroheliometer is described in detail by Kuzin *et al.* [2005].

Note that insignificant depressions, which can be related to a decreased emission measure in the dimming region, are observed in certain lines with an excitation temperature of about 1 MK (SiIX 296 Å, SiVIII 315 Å, etc.) in spectrum 2. Accurate quantitative estimates require statistical treatment of a signal.

2.3. Solar Activity Dynamics according to RATAN-600 Observations

The RATAN-600 radiotelescope was used in the daily observations in the wave band 1.83–15 cm performed from 0700 to 1100 UT on November 2–11, 2004. This period was characterized by activity in the flare-productive active region (FPAR) 10696, which generated two X-class X-ray flares. The FPAR radio emission was relatively stable. Activity increased at a level of several M-class flares on November 2–7, which resulted in the generation of an X2.0 flare at 1540 UT on November 7. The second period of activity resulted in the generation of an X2.5 flare at 0204 UT on November 10.

In the H_{α} line, the sunspot structure of the region was complex. In spite of this complexity, the magnetic structure varied monotonically when the region was located on the disk (Fig. 7). Activity of the first period caused high geomagnetic activity on November 8–11, and (according to the *Kp* and *Dst* indices) a decrease in activity on November 9 is related to the interval between M9.3 and M5.9 flares that occurred at 0011 and 0043 UT, respectively, on November 6 and an X2.0 flare observed at 1540 UT on November 7. An X2.5 flare that occurred at 0159 UT on November 10 resulted

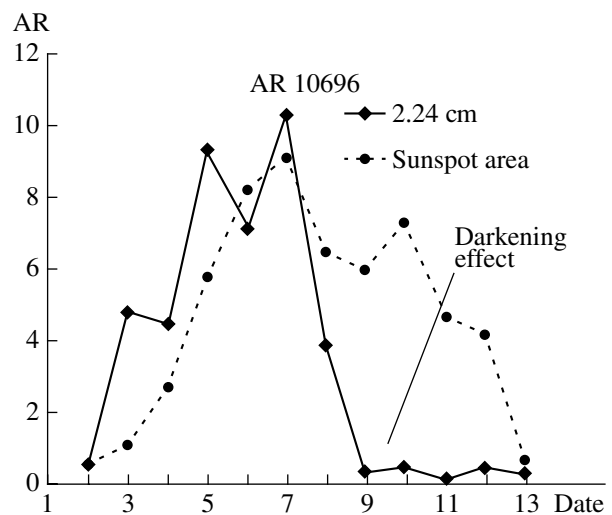


Fig. 10. Darkening effect in AR 10696 before the M2.5 flare of November 10, 2004. Dots show a change on the Sunspot area in the group at the level of the photosphere. Solid line corresponds to the total emission flux from AR 10696 at a wavelength of 2.24 cm.

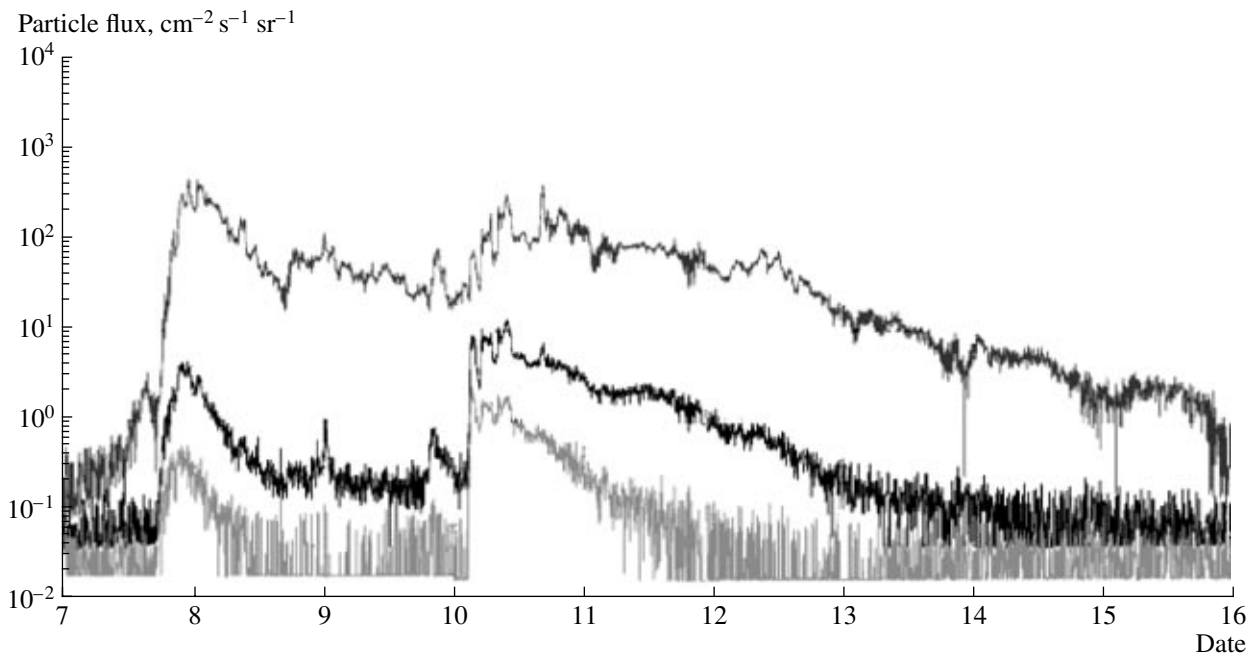


Fig. 11. Fluxes of protons with energies higher than 100, 50, and 10 MeV (curves from bottom to top) according to the GOES-11 observations during November 7–15, 2004.

in an insignificant increase in geomagnetic activity on November 13.

Bogod and Tokhchukova [2003] and Bogod *et al.* [2003] indicated that plasma manifestations in the spectrum of the FPAR microwave emission before a flare are various. Different effects in the spectrum of the polarized emission flux are especially pronounced. Although FPAR 10696 was stable, these effects were also clearly defined three days before a powerful flare in this region. Figure 8 presents the spectra of the polarized flux in this region on November 2–11, 2004. It is clear that the polarized flux started increasing in the HF zone of the microwave band (the arrow marks 13 GHz) beginning from November 4. As is known, this is related to the appearance of a new magnetic flux in an active region, which usually results in the generation of powerful flares. The polarized flux at these frequencies increased up to a powerful X2.0 flare that occurred at 1540 UT on November 7 and started decreasing after this event.

Sharp reversals of the circular polarization over the microwave emission spectrum were observed on November 7 several hours before an X2.0 flare (see Fig. 9). These changes indicate that the processes of primary energy release arised in FPAR immediately before a powerful flare.

The flare preparation scenario was different during the second period of activity. A sharp decrease in the emission flux on November 8 and 9 shown in Fig. 8 is apparently related to the origination of a darkening effect. Figure 10 demonstrates a change in the total radio flux at a wavelength of 2.24 cm during the entire

period of observations (November 1–13, 2004), which is comparable with the sunspot area in this active region. It is evident that the radio flux started decreasing much more abruptly than the total sunspot area after November 7.

Tokhchukova and Bogod [2003] analyzed similar darkening effects when they studied a powerful Bastille flare that occurred on July 14, 2000. The origin of this effect has not yet been determined in full and is possibly related to the radio propagation through a dense overlying plasma [Zlotnik, 2001]. The above data on the darkening effect and the model calculations indicate that hot plasma interlayers are probably generated on the emission propagation path. Protuberances and filaments that form CMEs can be such interlayers.

3. OBSERVATIONS OF THE HELIOSPHERE

3.1. Parameters and Events in the Solar Wind

In contrast to the last-year situation, when large fluxes of energetic particles caused serious failures in the operation of devices that measured parameters of the interplanetary medium on spacecraft (see, e.g., [Veselovsky *et al.*, 2004; Yermolaev *et al.*, 2005]), increases in the fluxes of energetic particles observed at the end of November 7 and at the beginning of November 10, 2004, were not so dramatic (see Fig. 11), and the complete sets of data on the solar wind (SW) and IMF were obtained (see Fig. 12). Figure 12 evidently demonstrates that the values of all plasma parameters (velocity V , temperature T , and density N) were not extreme in November. At the same time, the values of B

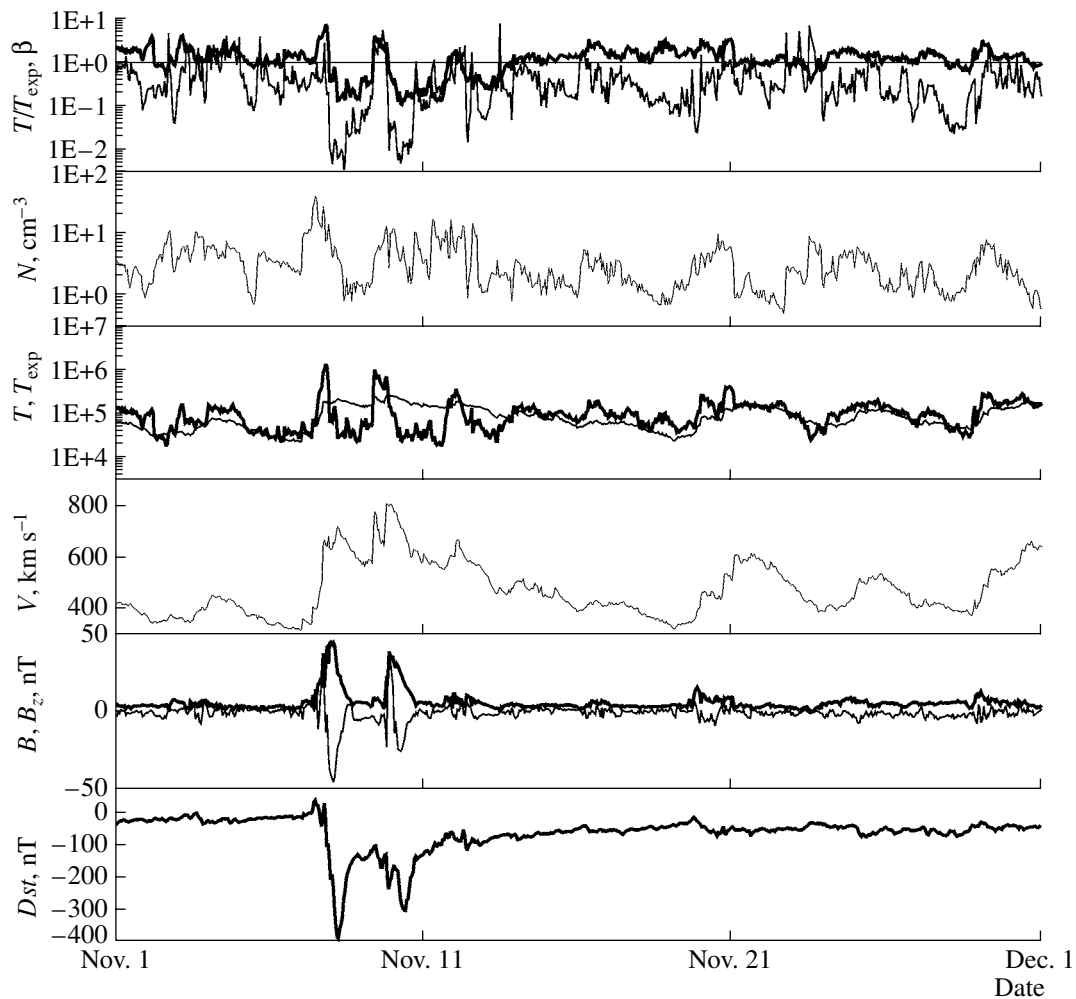


Fig. 12. Interplanetary medium parameters according to the satellite measurements in November 2004 in addition to the geomagnetic indices and X-ray measurements illustrated in Fig. 1.

Panel 1: parameter β (the ratio of the thermal and magnetic pressures, thin line) and the ratio of the proton temperature to such a temperature calculated from the average dependence of temperature on velocity, T/T_{exp} (thick line).

Panel 2: density, N .

Panel 3: proton temperatures T (thick line) and T_{exp} (thin line).

Panel 4: solar wind velocity, V .

Panel 5: IMF magnitude B (thick line) and B_z component (thin line).

Panel 6: Dst index.

and IMF B_z component reached extremely large values (>45 and -45 nT, respectively) on November 8, precisely which resulted in the generation of the strongest magnetic storm.

An analysis of Fig. 12 makes it possible to preliminarily conclude that the studied time interval was characterized by strongly disturbed conditions in the solar wind. Thus, six interplanetary shocks (see Table 4) and several magnetic clouds (interplanetary coronal mass ejections ICMEs) were observed on November 7–11. The beginning of the first magnetic cloud was registered at 2300 UT on November 7, which manifested itself, e.g., as a sharp decrease in the parameters β and

T/T_{exp} . The interplanetary shock (1800 UT) and the sheath region (characterized by increased temperature, density, and magnetic field magnitude) were observed before this cloud. In this case the negative B_z component appeared at 2000 UT; i.e., the magnetic storm was most probably caused by the sheath region before the cloud with a large negative B_z component rather than by the cloud itself. Since the IMF southward component was also observed at the beginning of the cloud, the Dst minimum was reached at 0600 UT on November 8. This cloud proved to be of short duration since it was overtaken by the other cloud or even by two clouds: shock waves at 0900 and 1700 UT (identification of

Table 4. Relation between solar events and interplanetary shock waves (ISWs)

Ord. no.	CME				Flare								Comments
	Date, t_k (UT) 2004	d°	Limb (Λ_0), deg	V_k , km s ⁻¹	195Å t_B , UT	195Å 1-8Å Peak	195Å Coordinates	H-alpha Flare class	Date, t (UT) 2004	Date, t_c (UT) 2004	V_{max} , km s ⁻¹	V_c , km s ⁻¹	
	1	2	3	4	5	6	7	8	9	10	11	12	13
1a	Nov. 3 0354	90	E, N30	800	Nov. 3 0336	M1.5	E45 N03	1N	–	Nov. 5 2300	–	400	$d/2 \leq L$ Impulsive
1	Nov. 3 1554	110	E, N32	800	Nov. 3 1524	M4.7	E37 N04	SN	Nov. 7 0257	Nov. 6 1324	365	400	$d/2 > L$ Impulsive
2	Nov. 4 0954	–	–	550	Nov. 4 0900	C6.0	E27 N03	SF	Nov. 7 1052	Nov. 7 1300	420	550	Partial halo CME Gradual
3	Nov. 5 0030	–	E N00 N70	720–1100	Nov. 4 2142	M5.5	E18 N05	1N	Nov. 7 1800	Nov. 7 0200– Nov. 8 0003	570	360–550	“Halo” CME Impulsive
4	Nov. 6 0131	–	–	650	Nov. 6 0000	M9.3	E04 N04	2N	Nov. 9 0900	Nov. 9 0800	800	650	“Halo” CME Gradual
5	Nov. 7 1331	–	–	1800	Nov. 7 1510	X2.0	W13 N03	–	Nov. 9 1812	Nov. 9 2300	800	900	“Halo” CME Impulsive
6	Nov. 8 0406	–	–	580	Nov. 8 0300	C8.0	W28 N03	SF	Nov. 11 1640	Nov. 11 1700	590	580	“Halo” CME Impulsive
7	Nov. 9 1726	–	–	550	Nov. 9 1700	M8.0	W45 N05	2N	–	Nov. 13 0900	–	560	“Halo” CME $d/2 \leq L$ Gradual

Notes: (1) The first appearance of CME in the LASCO C2 field of view, (2) CME angular dimension, (3) observation limb and visible latitude of CME origination site, (4) maximal plane-of-sky CME velocity, (5) time of X-ray flare beginning, (6) X ray class of a flare, (7) flare class in the $H\alpha$ line, (8) flare coordinates in the 195 Å line, (9) observed time of arrival of the sporadic stream (or shock) front in the Earth orbit, (10) calculated time of arrival of the sporadic stream (or shock) front in the Earth orbit, (11) observed maximal velocity immediately behind a shock front, (12) calculated maximal velocity immediately behind a shock front, (13) comments about CME.

Table 5. Certain parameters during Forbush decreases on November 7–11, 2004

FD	Date	UT (SSC)	Max. AR	Max Axy (eclipt. comp.)	SW velocity (V , km s ⁻¹)	IMF (B , nT)	VB	A_{FE}	Kp	Dst index, nT
1	Nov. 7	0257	0.6%	0.86%	366	7.2	1.32	0.5%	3	–5
2	Nov. 7	1052	0.4%	0.74%	414	11.3	2.34	0.7%	5–	10
3	Nov. 7	1827	7.3%	2.91%	726	45.7	16.58	7.5%	9–	–373
4	Nov. 9	0930	8.1%	3.98%	813	39.7	16.13	7.3%	9–	–289
5	Nov. 11	1710	1.1%	1.93%	673	12.2	4.11	1.5%	5	–113

solar wind streams between these shocks is rather difficult and ambiguous) and the leading edge of the cloud at 2100 UT on November 9. At the same time, the southward IMF component started increasing at 0100 UT on November 10. Therefore, the second mag-

netic storm was caused in this case by field variations in the magnetic cloud.

To determine the relation of interplanetary events to their sources on the Sun, we performed a preliminary analysis using the CME observations with the help of

the LASCO coronagraph on the KASOHO spacecraft in order to estimate the ejection velocity in the coronagraph field of view. For impulsive CMEs, the velocity of which V_k in the limb plane was higher than 750 km/s, we used the following formulas in order to determine the maximal velocity (V_{\max}) of the sporadic stream immediately behind the shock front in the Earth orbit and the time (Δt) of shock motion from the Sun to the Earth [Eselevich and Eselevich, 2004]:

$$V_{\max} \approx V_k/2 \quad (1)$$

$$\Delta t \approx 287R_{\odot}/V_k \approx 5.6 \times 10^4/V_k \text{ (km s}^{-1}\text{) [hours].} \quad (2)$$

For gradual CMEs, the velocity of which slowly increases to $V_k \approx 400\text{--}750$ km/s at $R \approx 30 R_{\odot}$ [Cane *et al.*, 1986] with increasing distance from the Sun and then remains approximately constant up to the Earth orbit, we have [Sheeley *et al.*, 1985a]:

$$V_k(R \approx 30R_{\odot}) \approx V_T \approx V_{\max}. \quad (3)$$

The estimates of the transport time (Δt) obtained using the formulas from similar works (e.g., [Cane and Richardson, 2003; Dal Lago *et al.*, 2004]) differ from the above estimates by $\pm 15\%$, which is within the accuracy of CME velocity measurement based on the LASCO data and of approximating curves. We also took into account that CMEs with $V_k < 400$ km/s do not generate a shock [Sheeley *et al.*, 1985b].

In the Earth orbit, six shocks labeled in Fig. 14 by S1–S6 were registered on November 7–11, 2004. Storm sudden commencements (SSCs) were observed on the Earth for five of these shocks (except S5). Eight CMEs (1a, 1–7), for which X-ray (marked by 1a, 1–7 in Fig. 13) and UV bursts were observed on the solar disk, were registered from November 3 to November 8. The times of beginning (t_B) of these flares, class of X-ray flares, and coordinates of UV bursts are given in Table 4. Three of seven CMEs were gradual, and the remaining CMEs were impulsive (Table 4, column 13). The nos. of the interrelated flares, CMEs, and shocks (Ss) are marked by the same numerals: 1–6. Shocks were not observed for CME 1a, 7 (see below). The measured values of t_B and V_k were used to find the correspondence between CMEs and shocks in the Earth orbit from the formulas (1)–(3). For shocks 1, 2, 4, 5, and 6, the calculated time (t_c) of shock front appearance at the Earth orbit agrees with the observed time (t) to within not more than ± 12 h (Table 4, columns 9, 10), and the calculated (V_c) and observed (V_{\max}) velocities are in agreement to within not more than ± 130 km/s (Table 4, columns 11, 12). For a halo CME3, two V_k values are shown for different o directions (Table 4, column 4). These values were used to calculate the minimal and maximal t_c values (column 10). The observed t value (column 9) is between these extreme values. Two CMEs (1a and 7) did not cause shocks in the Earth orbit because the ejection halfwidth was less than the CME source longitude ($d/2 < |L|$); therefore, the fronts of the related shocks apparently passed over the Earth.

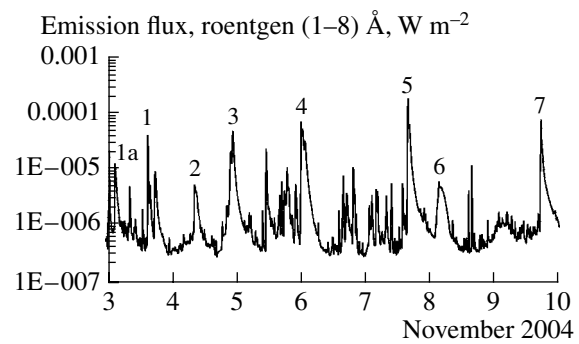


Fig. 13. Solar X-ray emission (1–8 Å) according to the GOES-12 data on November 3–10, 2004, and nos. of flares identified with ISWs on the ACE spacecraft (see Fig. 16).

As is known, the minimal southward IMF B_z component is the main parameter of the interplanetary medium responsible for a Dst value (see, e.g., [Akasofu *et al.*, 1985]). In this case it is important to note that the formula of relation between $\min Dst$ and $B_{z\min}$ depends on the degree of isolation of the considered stream. A sporadic stream that leads another sporadic stream by not less than 40 h should be considered non-isolated [Eselevich and Fainshtein, 1993]. For an isolated sporadic solar wind stream, $\min Dst$ and $B_{z\min}$ values can be estimated from the simple relationship [Akasofu *et al.*, 1985]:

$$\min Dst \text{ (nT)} \approx -7.8|B_{z\min} \text{ (nT)}| + 10 \text{ (nT)}. \quad (4)$$

Similar relationships for magnetic clouds were obtained in many works (see, e.g., [Wu and Lepping, 2002]). For non-isolated (following one after another at a short time interval) streams, the effectiveness of the impact on the Earth's magnetosphere is almost twice higher [Sheeley *et al.*, 1985b]. In spite of the fact that all streams are non-isolated in our case, the $\min Dst$ values observed for streams 3 and 5 (about -373 and -289 nT) satisfactorily fit the estimates (about -340 and -210 nT) obtained from the formula (4) for isolated streams but are slightly larger than the latter values.

The $Dst(t)$ dependence during the storm period November 7–12 is non-monotonic and shows a number of maximums and minimums in addition to two main minimums corresponding to two large magnetic clouds. The known regularity in the geomagnetic storm development is clearly defined [Akasofu *et al.*, 1985; Gonzalez *et al.*, 1999, 2004]: the time intervals when the IMF northward–southward components are negative and positive coincide with an increase and decrease in disturbance, respectively. The number of such intervals on the time profile of the above index is about ten during the considered period, and all of them correspond to the condition of interruption or delay of geomagnetic storm development [Veselovsky *et al.*, 2005].

We should note that the above description of the possible disturbance sources on the Sun corresponds to the old tradition and attempts to localize or relate the

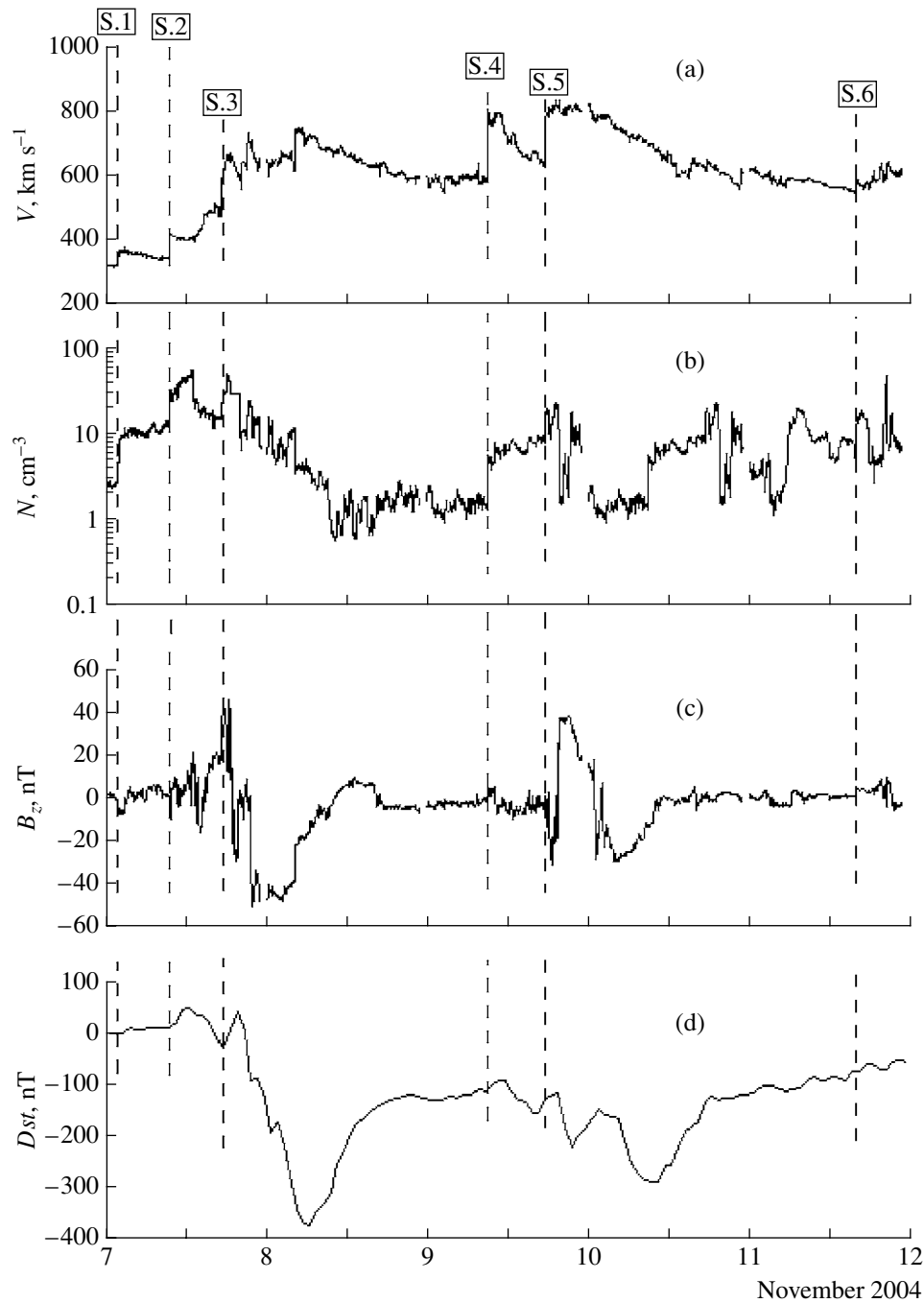


Fig. 14. Certain generalized parameters of the solar wind at 1 AU (ACE) and of magnetospheric disturbance during the considered period of November 7–11, 2004: (a) velocity, (b) density, (c) IMF B_z component, and (d) D_{st} index of geomagnetic activity.

causes of geomagnetic storms only to the processes in some active region. Basically the same analysis was performed in the preliminary reports and descriptions of the events considered here [Zhukov *et al.*, 2004; Yurchyshyn, 2004], where attention is also paid to flares and other processes in AR 10696. It is clear that such a priori localization is slightly conditional.

In reality one cannot rule out that the considered largest events in the heliosphere were also related to

and generated by the larger-scale structures and processes in the solar atmosphere, which were, in particular, transequatorial [Veselovsky *et al.*, 2005] and were in full measure caused by multiple CMEs with magnetic fields and electric currents. These ejections are clearly defined as global occultations on the disk and limb (shown on the difference images observed, e.g., at 1646:54–1546:54 on November 7 in the field of view of the EIT/SOHO telescope) and in the following devel-

opment of halo in the field of view of the LASCO coronagraphs. The ejections cover large sectors on the Sun including several active regions near the central meridian and in the southwestern part of the disk. This is also shown in the disappearance of a transequatorial loop protuberance, which is clearly defined in the successive images obtained in the H-alpha line at Kanzelhöhe solar observatory. The coronal magnetic field, calculated by G. V. Rudenko from the solar magnetograms in different approximations, also evidently demonstrates that large dynamic loops and the non-local dynamic relation between different active regions exist in this case. Moving and rapidly ejected inclined transequatorial magnetic loops, which were initially located between ARs 10696 and 10695 and had the initial scale of about a solar radius, are also observed on the EIT/SOHO movies.

Taking into account the results of the previous studies of the extreme events observed on the Sun and in the heliosphere in 2003, when the effective complex on the Sun also occupied at least three active regions on the visible side of the Sun, we can more confidently speak about the Sun's asymmetry (active longitudes) and about the global character of the considered increases in solar activity responsible for the strongest and multiple disturbances in the heliosphere. The transequatorial character of ejections can be related to the fact that, at the end of a solar cycle, active regions appear at low latitudes near the equator.

Finally, we should note that the prognostic centers gave confident and quite justified warnings of the possibility of strong geomagnetic storms during the considered period only when halo ejections were already registered in the field of view of the LASCO/SOHO coronagraphs and the ejection parameters were determined using (among other techniques) the dedicated, very promising, and updated computer aided CME tracking system (<http://sidc.oma.be/cactus/scan/output/2004/11/latestCMEs.html>). However, when the active regions appeared from behind the eastern limb, i.e., several days before the considered events, the Sun was quiet and low or moderate activity was anticipated during the entire solar rotation from November 3 to November 29. This prediction is considered in more detail in SWO PRF 1522 of November 2 (<http://www.sec.noaa.gov/weekly/pdf/prf1522.pdf>).

3.2. Interplanetary Scintillations

During the discussed period, scintillations were observed at a frequency of 111 MHz using the working model of the 16-beam pattern of the large scanning antenna (LSA), FIAN, Pushchino. The radio emission in the sky band 28° – 34° with respect to declination was registered around the clock. Information was obtained at an interval of 10 Hz at a characteristic time of 0.5 s. Such parameters of the receiving equipment make it possible to reliably register interplanetary scintillations of radio sources and slower ionospheric scintillations.

In this season it is possible to observe interplanetary scintillations of a relatively small number of sources because of a short daytime, high level of the background emission from the Galaxy plane, and low Sun.

When the LSA FIAN antenna was used to observe scintillations, the disturbances related to the active processes on the Sun on November 6–7, 2004, were registered at different instants in the interplanetary plasma and ionosphere. According to the delay time, these disturbances can be identified with two strongest flares observed in the X-ray emission as M9.3 (0038 UT on November 6) and X2.0 (1540 UT on November 7) events.

An M9.3-class flare resulted in considerable increases in the level of interplanetary and ionospheric scintillations in the evening of November 7 and at night of November 8. Nighttime scintillations of the 3C 48 radio source, which was observed at about 1930 UT on November 7, intensified. At that time the angle between the line of sight and the direction toward the Sun was more than 90° , and the source emission propagated through the near-Earth region of the solar wind. Scintillations were rather fast (the characteristic time was about 2 s), which indicates that they were related to the solar wind inhomogeneities. The value of the scintillation index, which characterizes the relative level of source intensity fluctuations, was several times as large as the corresponding value under quiet conditions. For compact radio sources close to 3C 48, increased interplanetary scintillations were not observed before 1930 UT. Two–three hours after 1930 UT, ionospheric scintillations considerably increased (characteristic times of about 10 s) for almost all observed sources, in particular, for 3C 115, 3C 123, and 3C 131 (for the first of them, ionospheric origin of scintillations follows from slow fluctuations; two latter sources do not scintillate on solar wind inhomogeneities owing to large angular dimensions). The level of ionospheric scintillations was also low before 1930 UT, which is confirmed by, e.g., the record of the Cas.A source at about 1800 UT. Summarizing the presented data, we can state that the disturbance caused by an M9.3 flare appeared near the Earth at about 1930 UT. In this case the delay time (t_0) relative to the flare instant was about 43 h, and the average velocity of disturbance propagation from the Sun to the Earth was not lower than 970 km/s. The SOHO proton monitor also gives similar estimates, according to which the disturbance delay time is approximately 42 h.

Qualitatively similar disturbances related to an X2.0 flare were observed by LSA on November 9, 2004. However, in contrast to an M9.3 flare and owing to the experiment specificity, we failed to determine rather exactly the disturbance time of arrival in the studied region of the interplanetary space. The increased level of interplanetary scintillations was registered at about 0700 UT for the 3C 286, 3C 293, and 4C+32.44 radio sources, which sounded the interplanetary plasma at a

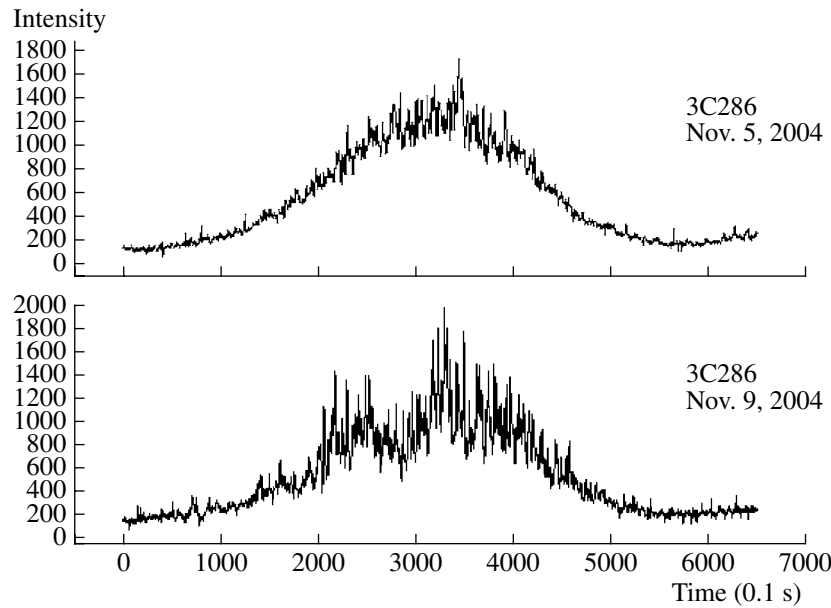


Fig. 15. Example of records of 3C286 interplanetary scintillations.

heliocentric distance of about 0.8 AU. Figure 15 illustrates the records of interplanetary scintillations for the 3C 286 source. It is evident that the scintillation level for the disturbed period of November 9 was substantially higher than for the quiet period of November 5. Scintillation enhancement on November 9 was sufficiently prolonged and continued to at least 1100 UT according to scintillations of the 3C 357 source (the studied region at a distance of 0.85 AU from the Sun) which was observed at that time. The above data indicates that the disturbance propagation time (t_0) from the Sun to 0.8 AU was not shorter than 39.5 h and the average velocity was higher than 850 km/s. Increased ionospheric scintillations were observed in the evening of November 9 and on the night of November 9–10. The disturbed state of the ionosphere followed into November 10. We should note that the solar radio flux at a frequency of 111 MHz on November 6–7 was increased but not so prolonged as, e.g., during the events at the end of October–beginning of November 2003.

The estimated times of shock propagation from the instants of flares to the sounding region of the medium are in good agreement with the estimated propagation times of corresponding CMEs (Table 4) and, on the other hand, make it possible to determine the initial velocities of shock waves generated by these CMEs. The dependence of a wave velocity V on a heliocentric distance r can be described by the power function

$$V(r) = V_0(r/r_0)^{-n}, \quad (5)$$

where the value $r_0 \approx 0.2$ AU can be taken, and the exponent n varies within the limits $1/2 \leq n \leq 1$ [Parker, 1961; Dryer, 1984; Vlasov, 1988; Chashei and Shishov, 1995]. The calculations indicate that the model maxi-

mal propagation velocities of both shocks varied from 1000 km/s (at $n = 1/2$) to 2000 km/s (at $n = 1$); i.e., the initial model shock velocities are slightly higher than the velocities of corresponding CMEs measured by the LASCO/SOHO coronagraph. In this case the best agreement is reached at $n = 1/2$ for the flare of November 6 and at $n = 1$ for the flare of November 7 (Table 4).

3.3. Solar Cosmic Rays

Solar cosmic rays (SCRs) generated by solar flares at the end of October–beginning of November 2004 were registered in the near-Earth space by the equipment installed on the CORONAS-F satellite. This satellite is the Russian space solar observatory designed to study nonstationary processes on the Sun and their effect on the interplanetary medium and the Earth's magnetosphere. The second satellite of the CORONAS series represents the low-altitude spacecraft with an initial orbit height h_{orb} of about 500 km (in November 2004 the orbit height was approximately 400 km), an inclination i of 82.5° , and a orbiting period (T_{orb}) of 94.5 min [Kuznetsov *et al.*, 1995, 2002]. The results of solar flare registration obtained during the period of high flare activity in October–November 2003 are considered in detail by Panasyuk *et al.* [2004] and Yermolaev *et al.* [2005].

Moving along its trajectory, CORONAS-F crosses polar caps, whose field lines stretch into the magnetotail and are almost open to SCRs; therefore, considerable differences in the obtained time variations in SCRs between the polar caps and solar wind, including the dependence on the time variations in IMF, are not observed.

Figure 16 demonstrates the time variations in the fluxes of solar protons and electrons in several energy channels of the MKL detector [Kuznetsov *et al.*, 2002] measured in the northern and southern polar caps during the period under study. Three SCR increases with maximums on October 30, November 1, and November 7 are clearly defined in Fig. 16. Unfortunately, a considerable gap (from November 10 to November 15) is present in the data of the MKL device because of the absence of telemetry; however, even the available data are of a certain interest from the viewpoint of studying the SCR dynamics. Let us consider these data in more detail.

According to the GOES data (<http://www.sec.noaa.gov/ftpd/indices/SPE.txt>), the SCR event of November 7 was caused by an X2-class flare that occurred on the Sun at about 1600 UT on November 7 in AR 10696, which was located at N09W17 at that time. Figure 16 indicates that this flare resulted in the most intense increase in SCRs with a rather hard spectrum during the considered period. However, we should note that the intensity of SCR protons in this spectrum was approximately one and a half orders of magnitude as low as the SCR intensity observed after the flares in October–November 2003 in the range of energies 1–5 MeV and two orders of magnitude lower for energies of 50–90 MeV. Maximal intensities of SCR electron fluxes in 2003 exceed SCR electron fluxes in 2004 by more than two orders of magnitude in the channel 300–600 keV and by three orders of magnitude in the channel 1.5–3 MeV [Panasyuk *et al.*, 2004]. We should also note that significant fluxes of electrons with energies higher than 6 MeV were not observed during the considered period of 2004 in the CORONAS-F experiment.

Figure 16 also indicates that a considerable (by an order of magnitude) increase in the flux of protons with energies of 1–5 MeV was registered by CORONAS-F on November 5–6 and, consequently, was caused by a flare that occurred before November 7. Figure 16a demonstrates that the fluxes of protons with energies of 14–26 MeV and higher started increasing only on November 7 after an X2 flare. We assume that this increase in SCRs of low energies could be caused by an M9.3 flare that occurred near midnight on November 4–5 in the same AR 10696 (N09E05). Figure 16b indicates that fluxes of electrons with energies higher than 3 MeV appeared together with protons with energies higher than 14 MeV, and an insignificant (by a factor of 3–4) increase in the fluxes of electrons in the channels 300–600 and 600–1500 keV, probably related to the earlier flare mentioned above, was observed on the previous two days.

An increase in the SCR fluxes observed on November 1 is presumably related to a flare that occurred behind the limb (<http://www.sec.noaa.gov/ftpd/indices/SPE.txt>). Figure 16a indicates that this SCR event had a very hard proton spectrum: the fluxes of protons with energies of 1–5 MeV registered during this event

were approximately one and a half orders of magnitude as low as during the next event, and the flux of protons with energies of 26–50 and 50–90 MeV was almost identical, as well as the flux of electrons with energies of 1.5–3 MeV, whereas the flux of electrons with energies of 3–6 MeV registered on November 1 was lower than during the next event by a factor of 2–3.

In our opinion, an insignificant increase in SCRs started at about 0500 UT on October 30 was related to an M3.3 flare that began on October 30 in AR 10691 (N13W20). Figure 16a demonstrates that the fluxes of protons with energies of 1–5 MeV are different in the northern (filled squares) and southern (crosses) polar regions during this event, which is presumably related to the asymmetry in the filling of the northern and southern polar caps and should be considered independently. The electron spectrum is much softer during this increase: the flux of particles with energies of 300–600 keV is higher than that of electrons with energies of 600–1500 keV by almost an order of magnitude, whereas these fluxes were almost identical during the event of November 1.

3.4. Galactic Cosmic Rays

The Forbush effect of October 29 and the geomagnetic effect of November 20, 2003, were the largest events for not only the current solar cycle (cycle 23) but also for the entire history of ground-based CR observations [Veselovsky *et al.*, 2004; Panasyuk *et al.*, 2004; Belov *et al.*, 2005a, 2005b; Yermolaev *et al.*, 2005]. When the Sun approached the cycle minimum, it had to decrease its activity; therefore, new powerful bursts of activity a year later (in November 2004 and in January 2005) proved to be rather unexpected.

The activity burst in November 2004 resulted again in significant sporadic CR variations, although the amplitude of these variations was smaller than during the events observed in 2003 or in March–April 2001. Figure 17 presents certain characteristics of the interplanetary medium and the behavior of CRs and geomagnetic activity on November 6–12, 2004. According to the NOAA data (<ftp://area.nrl.navy.mil/pub/lasco/halo>), partial or full halo CMEs occurred almost every day mainly from AR 10696, so that two–three disturbances, which as a rule generated shock waves, were constantly present in the interplanetary space. Figures 12, 14, and 17 indicate that several shocks reached the Earth for five days (five SSCs were registered; see Fig. 17, middle panel). Subsequent disturbances were accompanied by a sharp increase in the solar wind velocity (up to 700–800 km/s) and IMF enhancement (up to 40–45 nT) and resulted in considerable variations in geomagnetic activity: the *Dst* index decreased to –373 and –289 nT (see Table 4), and the *Kp* index reached 9– during the storms of November 8 and 10.

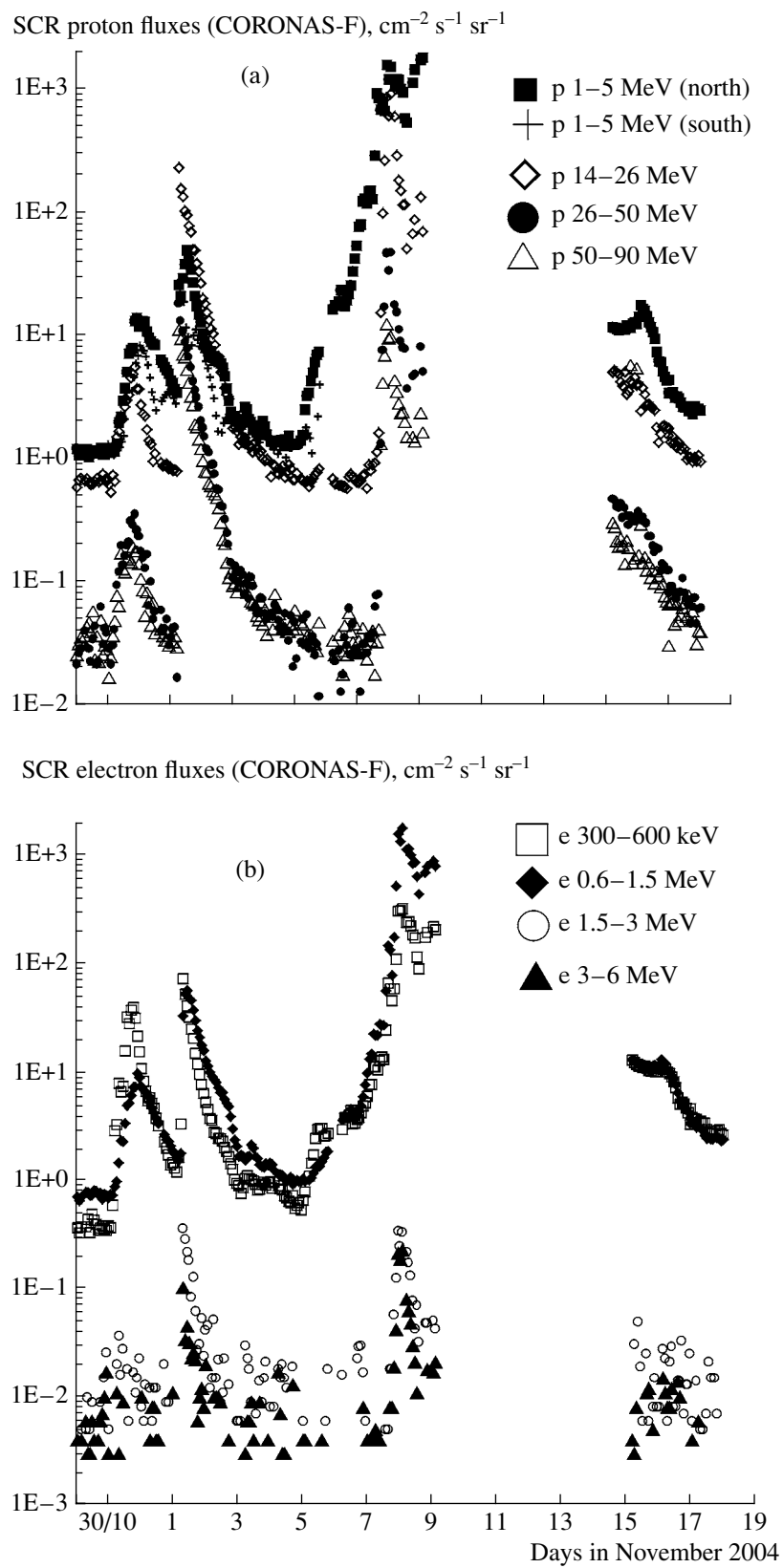


Fig. 16. Fluxes of (a) protons in both polar caps and (b) electrons in the northern polar cap from October 29 to November 18, 2004, according to the CORONAS-F satellite data.

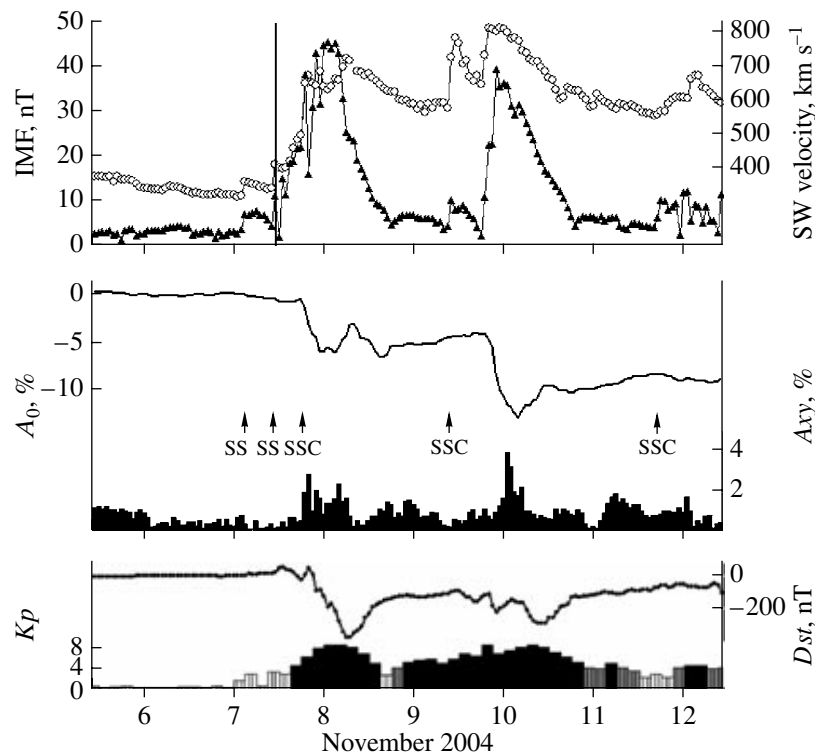


Fig. 17. Variations in the parameters of the interplanetary medium, CRs, and geomagnetic activity during the disturbed period of 2004: (A_0) CR density, (A_{xy}) ecliptic component of the anisotropy first harmonic of CRs with a rigidity of 10 GV, and (K_p) and (Dst) geomagnetic activity indices.

This situation was naturally reflected in the behavior of galactic cosmic rays (GCRs) in the form of Forbush effects (FEs). Figure 17 (middle panel) presents the variations in the density of CRs with a rigidity of 10 GV and in the equatorial (A_{xy}) component of the anisotropy first harmonic obtained by the global survey method (GSM) based on the data from the global network of neutron monitors. Table 5 lists the maximal values of Forbush decreases and the A_{xy} component for five Forbush decreases, as well as the main parameters of the interplanetary medium and the geomagnetic activity indices during the considered period. The data presented indicate that gigantic events similar to FE of October 29, 2003, were not registered during this period. Nevertheless, the series of FEs and the value and character of these effects indicate that the disturbance level was rather high for the solar cycle phase near minimum.

FEs after the third and fourth shocks with decreases of 7.3 and 8.1% (nos. 3 and 4 in Table 5) proved to be the most significant events. Belov *et al.* [2001] demonstrated that the Forbush effect value generally depends on the state of the interplanetary medium via the VB parameter (the product of the maximal solar wind velocity and the IMF strength during the considered event as compared to their values in the quiet wind). This parameter was calculated for the events of November 2004 and is also presented in Table 5. The values of

the maximal Forbush decrease amplitude (A_{FE}), obtained using the A_{FE} dependence on VB derived in [Belov *et al.*, 2001], are given in the next column of Table 5. It is clear that the calculated and directly obtained values are in rather good agreement. The maximal deviation of the actual decrease amplitude for event 4 is apparently related to the western disturbance source and to the better conditions of charged particle exchange between the FE region and the ambient interplanetary space.

The same events in CRs are presented in Fig. 18 in a slightly different form. The vector diagram in this figure indicates the behavior of the equatorial component of the CR anisotropy first harmonic. Thin lines drawn at equal time intervals join the same instants on the vector diagram and on the CR density time base; the vertical arrows correspond to the value and direction of the north–south anisotropy for each hour of the considered events. First of all, it is interesting that anisotropy substantially changes even during as if insignificant Forbush effects (Table 5, nos. 1, 2) with the amplitude $<1\%$: after several quiet days, the A_{xy} vector started sharply changing its direction from usual ~ 18 h to 12, 0, and 6 h after the arrival of the first shocks. During and after the third event, a considerable increase in the anisotropy amplitude (in both elliptic and north–south components) was accompanied by sharp changes in the anisotropy direction. The anisotropy behavior espe-

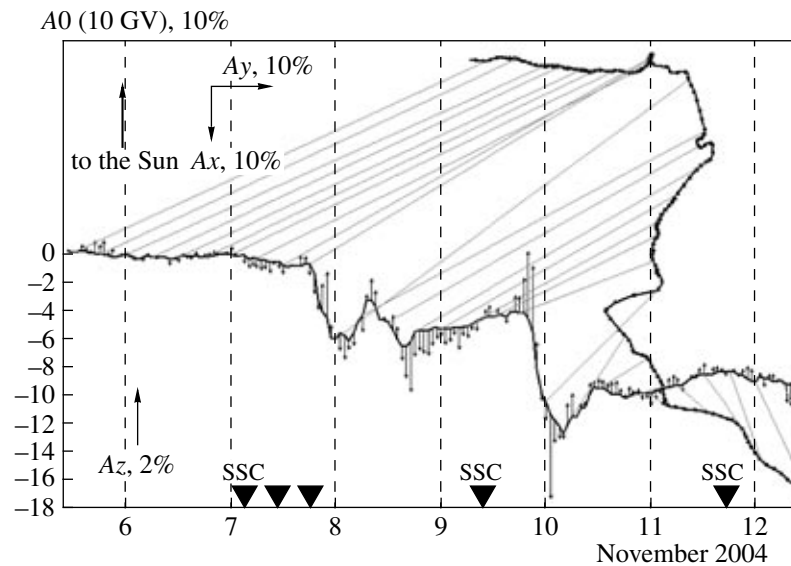


Fig. 18. Variations in the CR density (A_0) and anisotropy in the series of FEs in November 2004. The vector diagram presents the ecliptic component of the anisotropy first harmonic (A_{xy}), and the vertical arrows correspond to the north–south component. Triangles show the instants of shock arrival in the near-Earth space.

cially sharply deviated from such a behavior in the quiet period during events 3 and 4. Rapid changes in the solar wind and IMF during a disturbed period result in complicated structures that pass over the Earth and are reflected in the behavior of CRs even with energies observed by neutron monitors. At the observed solar wind parameters, the Larmor radius (ρ) is $\sim 8 \times 10^{10}$ cm for particles with a rigidity of 10 GV ($\sim 8 \times 10^9$ cm for 1 GV). At a wind velocity of about 730 km/s, a disturbance will cover the distance ρ over approximately 20 min, and CR changes at a distance of up to three–four Larmor radii will be present in hourly observations. Therefore, it is not surprising that such sharp hourly changes are observed in the CR anisotropy direction and amplitude.

An unusual feature in the CR density behavior was observed after the appearance of the fourth SSC at 0930 UT. A decrease in the CR density was not registered for 10 h after the shock arrival, although it is easy to observe the response in the anisotropy behavior. The absence of a considerable CR modulation can indicate that the disturbance which passed near the Earth at that time had an open structure. A considerable FE, as well as the strong magnetic storm, began only late on November 9 after the next jump of the solar wind velocity and IMF strength (not accompanied by SSC).

We can also note that the CR density behavior was slightly unusual on November 8 at the Forbush effect minimum (FE3). At that time the density increased (by about 2%) for approximately 12 h. The peak of this increase coincides with the solar wind jump and with the Dst variation minimum (-373 nT). It might seem that this should be the manifestation of the magnetospheric effect in CRs. However, an additional analysis

does not make it possible to unambiguously accept such an explanation. The magnetospheric effect as a rule manifests itself at middle- and low-latitude stations and is almost imperceptible at stations where a rigidity is $< 2\text{--}2.5$ GV. However, in this case the CR intensity increased at both middle- and high-latitude neutron monitors (except the easternmost ones) and even at polar stations (Fig. 19). The stations with the geomagnetic cutoff rigidity > 1.2 GV (with the most anticipated magnetospheric effect) were not treated by the global survey method, but this did not change the situation. Thus, this increase in density at the FE minimum could at least partially result from GCR modulation by certain structures in the interplanetary space. At that instant the next part of a disturbance propagated at a higher velocity than the previous part, and the compressed region with an increased CR density and a rather complicated structure (which manifested itself as sharp but short-term changes in CR anisotropy) originated as a result of the interaction between solar wind streams (Fig. 18).

During highly disturbed periods similar to the period under discussion, a pronounced intensification of GCR fluctuations is observed together with sharp changes in GCR density and anisotropy. Figure 20 includes results of the GCR monitoring from October 15 to December 10, 2004, at the Yakutsk Space Weather Center IKFIA (<http://ikfia.ysn.ru/fluctuations/index.php>). The results of calculating the GCR scintillation index based on 5-min GCR intensity values (in percent) are presented in relative units for two polar stations: Tixie Bay and Oulu (Finland). The 5-min values of the GCR scintillation index were subsequently averaged over 12 h. According to the definition given in [Tugolukov and Kozlov, 1991; Kozlov and

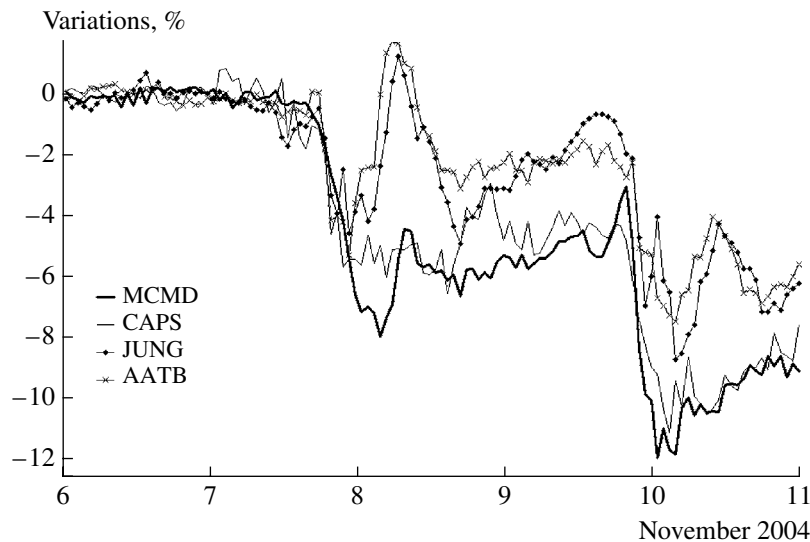


Fig. 19. Variations in the neutron monitor count rate relative to the base on November 6 at the stations: McMurdo (MCMD), $R_c = 0.01$ GV; Cape Schmidt (CAPS), $R_c = 0.52$; Jungfrauioh (JUNG), $R_c = 4.48$; Alma Ata 3300 m (AATB), $R_c = 6.69$ GV in November 2004.

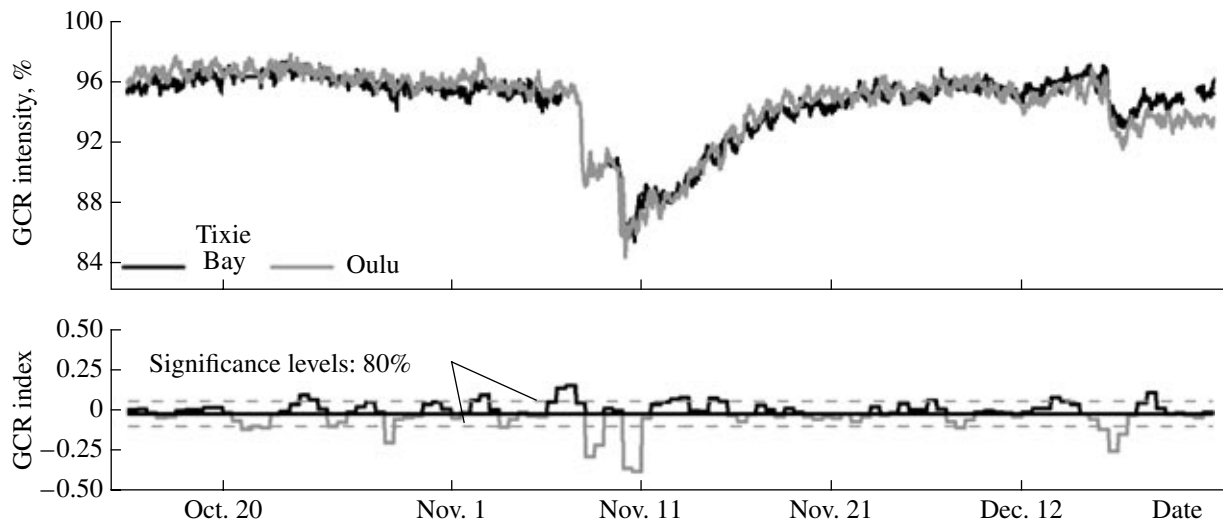


Fig. 20. Average hourly values of the GCR intensity (in percent) at Tixie Bay and Oulu (Finland) polar stations. Results of the effective prediction of the extreme events of November 7–9, 2004, based on the ground-level GCR monitoring using the 5-min data of the polar stations, are shown in the bottom part of the figure.

Tugolukov, 1992], the scintillation index corresponds to the index of a fluctuation frequency spectrum generalized by the authors to the case of noise-type processes. The spectral index is determined as a trend for the amplitudes of frequency spectrum harmonics using the criterion similar to the Kendall trend criterion [Bendat and Piersol, 1986].

Two dashed lines show the significance levels (80%) for the scintillation index, which are determined similarly to the significance levels for the trend according to the Kendall criterion. The GCR scintillation index val-

ues exceeding the upper significance level of 0.075 (80% level) correspond to the registration of a *predictor*. The scintillation index values below the lower significance level of -0.075 (also 80%) suggest event diagnostics. The universal time scale in days is plotted on the abscissa. The scintillation index becomes maximal on November 6–7, 2004, a day before the Forbush-effect beginning on November 7–9.

The GCR behavior, similar to the behavior shown in Figs. 19–20 for November 7–10, 2004, was also observed at Apatity station (Section 4, Fig. 32) and in

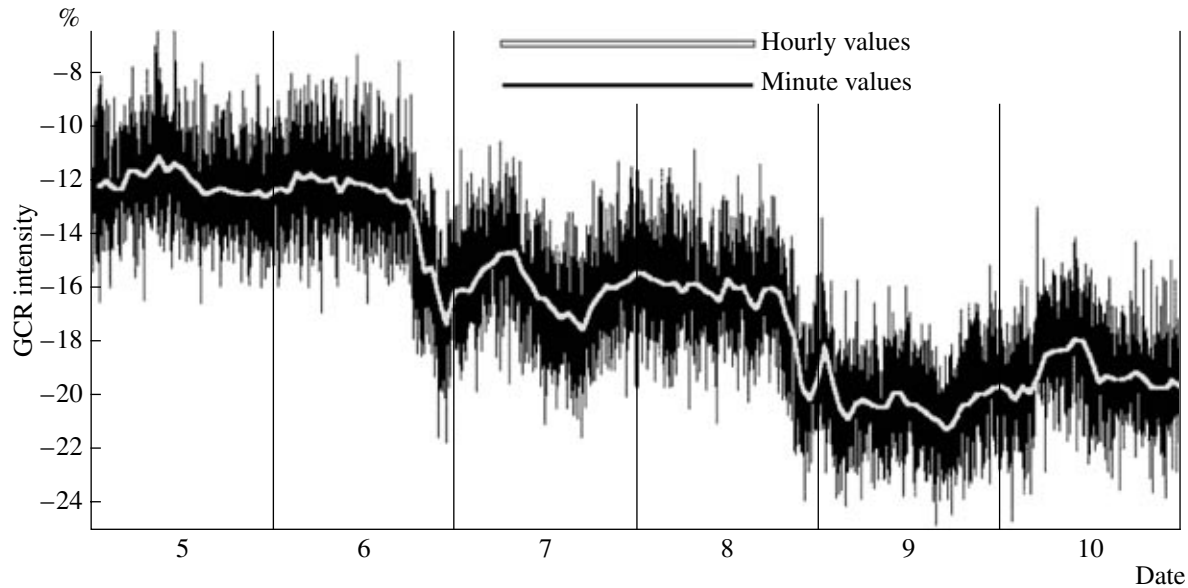


Fig. 21. Count rate of the 24-NM-64 Novosibirsk neutron monitor (minute and hourly values) on November 5–10, 2004.

Novosibirsk (geographic latitude $\lambda = 54.80^\circ$ N; geographic longitude $\varphi = 83.00^\circ$ E; height above sea level $h = 163$ m; see Fig. 21).

Table 6. List of the greatest ($ApD > 100$) magnetic storms during cycle 23

Date	ApD	Ap_{\max}	Kp_{\max}	Dst_{\min}	SSN
Oct. 29, 2003	204	400	9.0	-345	167
Mar. 31, 2001	192	300	8.7	-387	205
Oct. 30, 2003	191	400	9.0	-401	167
July 27, 2004	186	300	8.7	-182	55
July 15, 2000	164	400	9.0	-300	148
Nov. 10, 2004	161	300	8.7	-289	36
July 25, 2004	154	207	8.0	-150	57
Nov. 20, 2003	150	300	8.7	-472	90
Aug. 27, 1998	144	207	8.0	-155	100
Nov. 6, 2001	142	300	8.7	-292	140
Nov. 8, 2004	140	300	8.7	-373	57
Aug. 12, 2000	123	179	7.7	-237	170
Nov. 9, 2004	119	300	8.7	-223	52
Sept. 25, 1998	117	236	8.3	-207	105
Oct. 31, 2003	116	236	8.3	-320	160
Oct. 5, 2000	116	179	7.7	-192	128
May 29, 2003	109	236	8.3	-130	56
Aug. 18, 2003	108	154	7.3	-168	67
Nov. 24, 2001	104	236	8.3	-221	67
May 4, 1998	101	300	8.7	-205	73

4. MAGNETOSPHERIC OBSERVATIONS

4.1. Behavior of Geomagnetic Indices

On the whole, the magnetic storms in November 2004 were not only the greatest events of this year (Fig. 22) but are in the list of the largest magnetic storms during cycle 23 (Table 6). It is interesting that a half of this list includes the storms of October 2003–November 2004; i.e., the number of especially strong storms that occurred for almost one year is equal to the number of such events observed in the previous seven years.

Subsection 3.1 indicated that the equatorial geomagnetic field described by the Dst index was strongly disturbed and is adequately described by the observed parameters of the interplanetary medium and, specifically, by the IMF southward component. The magnetic storms of November 2004 were also characterized by very high geomagnetic activity at auroral and polar latitudes (higher than 2000 nT according to the AL index), which was comparable with such an activity value during the events of October–November 2003. A detailed analysis of the auroral electrojet dynamics can be performed later, when corrected results of observations of different magnetospheric parameters will be obtained; however, certain conclusions can be made based on the available preliminary data. Figure 23 demonstrates the variations in the IMF B_z component in the GSM coordinate system (upper panel); in the solar wind electric field calculated from the formula

$$E = V\sqrt{B_z^2 + B_y^2}/2\sin(\theta/2)^4 + \alpha V^2,$$

$$\alpha = 4.4 \times 10^{-6} (\text{mV m}^{-1})/(\text{km s}^{-1})^2,$$

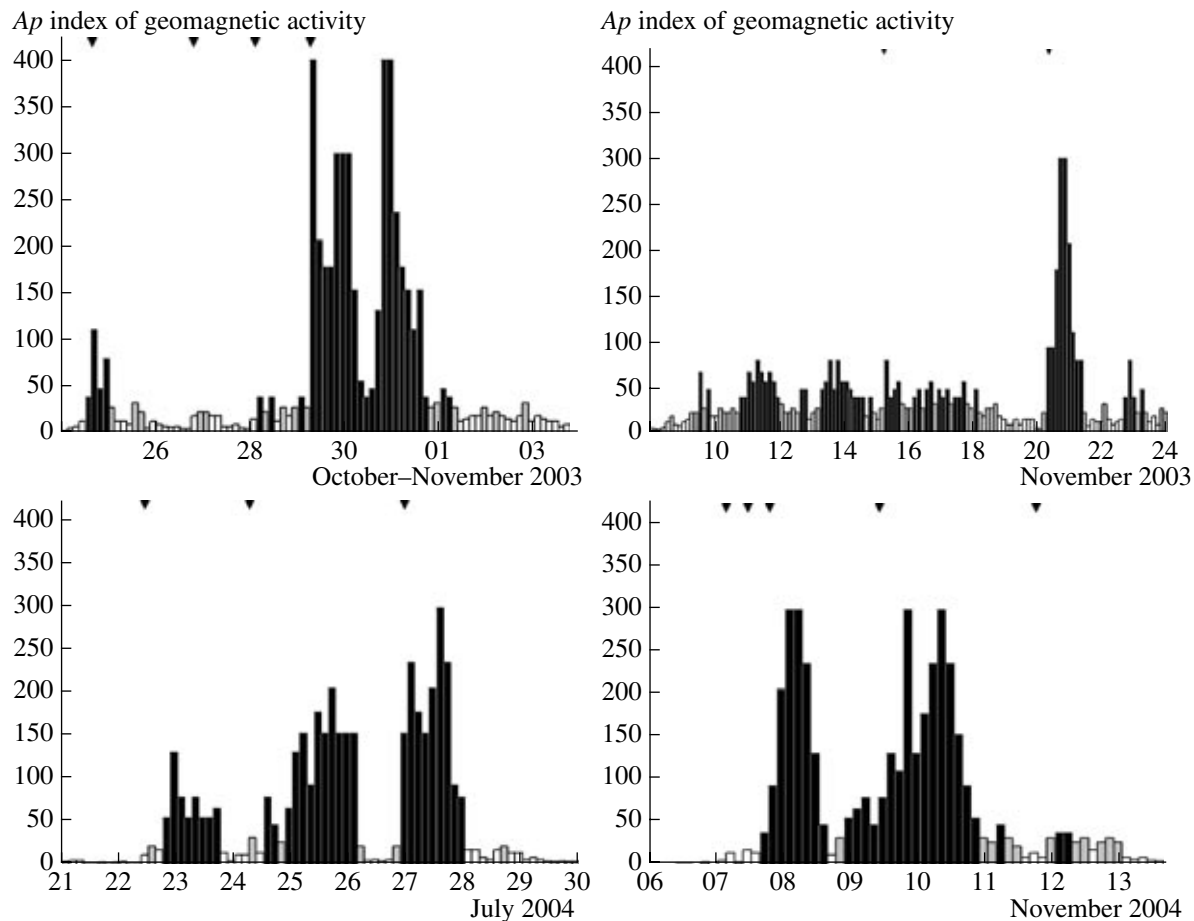


Fig. 22. Three-hour A_p indices during the extreme events of October 2003–November 2004.

where θ is the IMF clock angle (as was shown previously, the correlation between this combination of the solar wind parameters and the AL index is the best (see [Yermolaev *et al.*, 2005]) (middle panel); and in the AL index digitized based on the preliminary plot (lower panel).

During the considered event, the near-Earth solar wind velocity was almost twice lower than during the magnetic storms of October 2003 and was not higher than 1000 km/s. Therefore, the variation in the IMF southward component mainly contributed to the electric field value. In turn, the amplitude of variations in the AL index was also approximately twice lower (~ 1500 – 2000 nT). We should separately point to several short-term increases in auroral geomagnetic activity to ~ 4000 nT. Episodic variations in a similar amplitude are not unique and were also registered during weaker magnetic storms. For example, on September 25, 1998, when the value of the solar wind electric field was quite moderate (about 12 mV/m), the CANOPUS network of magnetometers registered the deviation of the horizontal component to the values of about ~ 4000 nT, which was, in particular, explained by specific features in the dynamics of the geomagnetic tail.

4.2. Geomagnetic Disturbances on the Earth's Surface

The intense magnetic storms of November 2004 occurred after the electromagnetic effect of a solar flare (solar flare effect, *sfe*) or *croshet* of November 6, 2004, which was generated by three M9.3 (0011 UT), M5.9 (0044 UT), and M1.4 (0140 UT) X-ray flares and by gamma bursts in the energy range 50–100 keV. *Croshet* and related *Psfe* geomagnetic pulsations are caused by an impulsive increase in ionization at altitudes of the D and E regions in the dayside middle- and low-latitude ionosphere [Mitra, 1974; Parkhomov, 1994]. The variations in the X-ray emission according to the HESSI satellite measurements are presented in Fig. 24 (panels a, b). Figure 24a indicates that the X-ray emission in the energy channels 1.6 and 3.1 keV started increasing at 0011 UT and reached its maximum at 0034 UT. The gamma emission began at 0013:32 UT, reached the maximum at 0032:18 UT, and ended at 0105:52 UT (Fig. 24b).

The geomagnetic response at two midlatitude observatories in the prenoon hours of MLT is shown in Figs. 24a–24e. Figure 24a demonstrates the fragment of the H component at Irkutsk observatory (0700 MLT). The

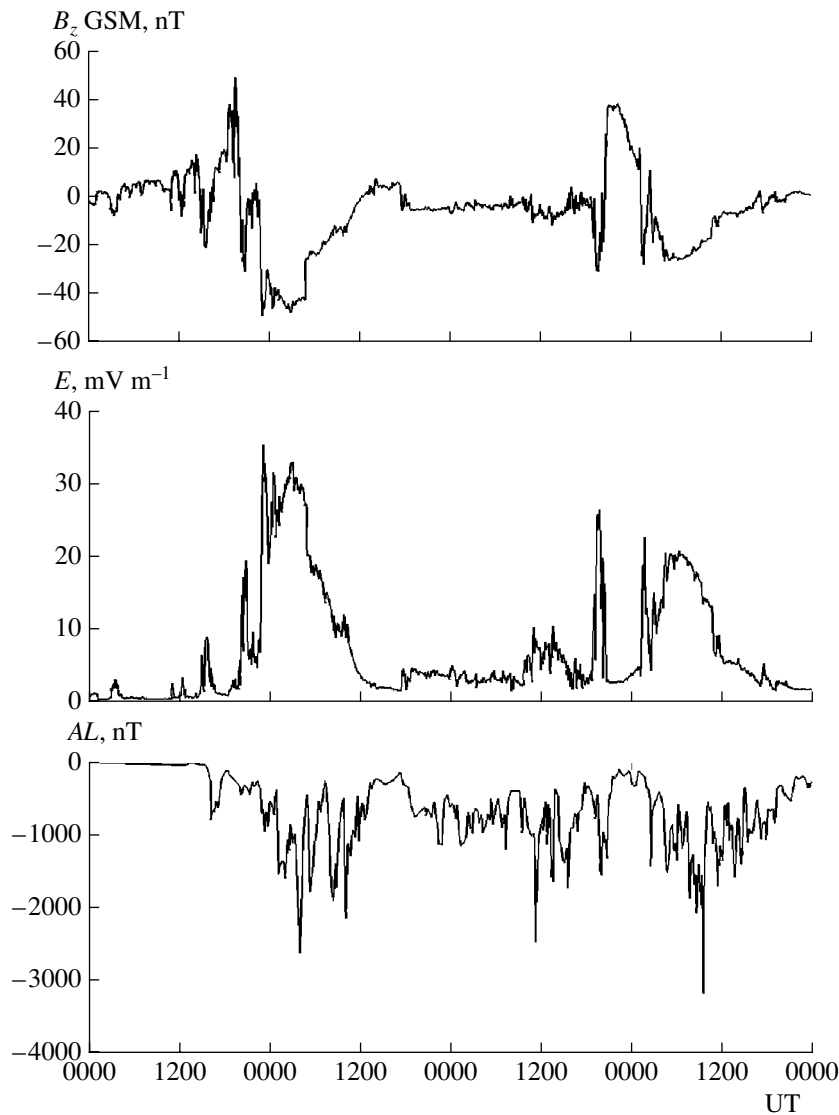


Fig. 23. The IMF B_z component in the GSM coordinate system, the SW electric field values (hourly average) measured on ACE and shifted in time with regard to the satellite distance from the Earth, and the preliminary AL index values (hourly average) for November 7–10, 2004.

beginning of the magnetic disturbance with an amplitude of ~ 4 nT coincided with the gamma emission maximum in the energy range 50–100 keV. Figure 24c presents the fragment of the H component at Kakioka observatory (0900 MLT). The analog records of geomagnetic pulsations at the same observatory, filtered in the P2sfe (50–250 s) and P3sfe (250–650 s) ranges of periods, are shown in Figs. 24d and 24e. The denotations and justifications of separating the pulsations into three types according to spectral singularities were considered in detail by Parkhomov and Lukovnikova [1983].

Let us consider the spatial distribution of the SFE effect currents, which are accompanied by impulsive geomagnetic pulsations according to data of the global network of stations. Figures 25a and 25b presents the

fragments of the standard magnetograms from several low- and middle-latitude observatories in different MLT sectors for the intervals of gamma-burst registration on (a) November 4, 2003, and (b) November 6, 2004. The interval of gamma emission observation and the instant of emission maximum are marked in Fig. 25 by open rectangles and an arrow, respectively. Solid vertical lines on the plots correspond to the instants of registration of gamma emission maximums. It is clear that a magnetic pulse is globally registered in all presented MLT longitude sectors to an accuracy of ± 1 min.

For the flare of November 4, 2003, the maximum in the H component (determined directly from the text file of data) was observed at 2041 UT at all stations in the dayside sector and at 2040 UT only at two stations in the postmidnight sector: IRT (0340 MLT) and KAK

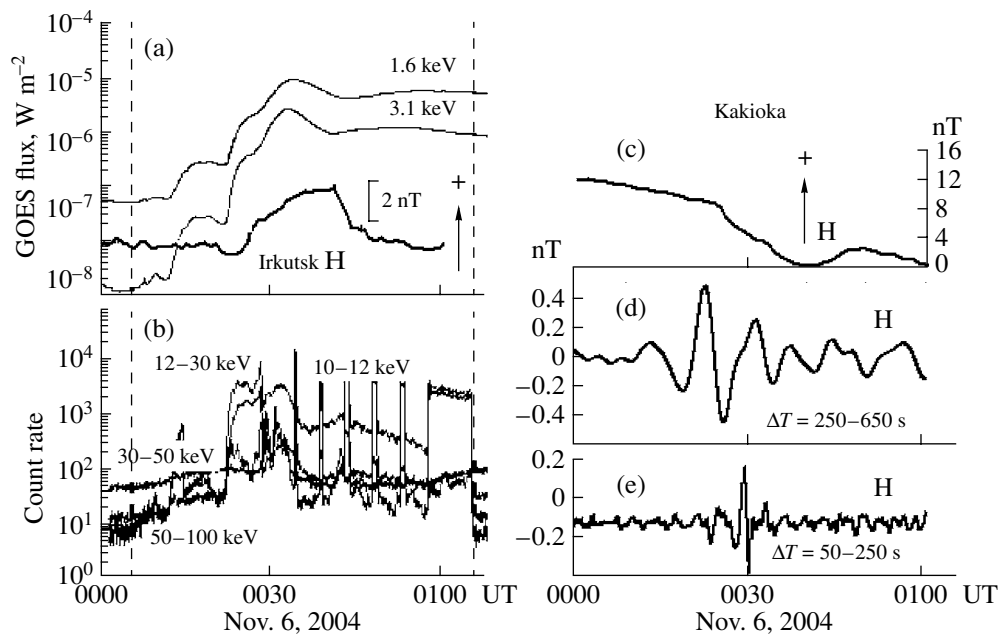


Fig. 24. (a) Variations in the X-ray flux with a quantum energy of 1.6 and 3.1 keV and the fragment of the geomagnetic field H component at Irkutsk observatory (IRT) accompanying the flare of November 6, 2004; (b) variations in the gamma-quantum count rate in four energy channels; (c) fragment of the geomagnetic field H component at Kakioka observatory; (d) variations in the H_x component of geomagnetic pulsations in the range of periods 250–650 s (P3sfe) at Kakioka observatory; and (e) variations in the H_x component of geomagnetic pulsations in the range of periods 50–250 s (P2sfe) at Kakioka observatory. Arrows with + indicate growth of an element.

(0540 MLT). The pulse maximal amplitude (~ 12 nT) was observed at HUA near-noon low-latitude observatory.

For the flare of November 6, 2004, the current maximum can be determined at 0040 UT at all stations except HON near-noon station (1300 MLT). The pulse maximal amplitude (~ 8 nT) was observed at KAK observatory. The pulse amplitude decreases toward the dusk and dawn sides but remain about 0.5–1 nT even at midnight stations.

It has been studied in detail that magnetic storms and their structural elements, especially preliminary impulses (PRI) of magnetic storm sudden commencement, are registered simultaneously over the entire globe. It has been found out that certain types of Pc5 oscillations, presumably caused by large-scale oscillations of the magnetosphere related to fluctuations of the field-aligned currents in the auroral zone, are also global (see, e.g., [Motoba *et al.*, 2002]). In the cases considered by us, the generation of magnetic impulses is related to the effect of hard electromagnetic emission on the ionosphere and to the ionization processes. In both considered cases, pressure pulses or sharp IMF changes, which could cause an increase in the auroral or magnetopause currents, were not registered in the solar wind. Substorms were also not observed in the considered intervals.

In our opinion, it is appropriate to propose the following hypothesis in order to discuss the observation

results. Moldavanov [2003] considered the favorable conditions for the generation of the electric field (with the magnitude close to the breakdown threshold) in a polarized layer, which is originated at atmospheric altitudes as a result of gamma emission absorption. A similar electric breakdown (stratospheric lightning) is the source of broadband emission of different physical origin (electromagnetic, acoustic-gravity, thermal, etc.), which can result in the generation of different-frequency oscillation processes. In particular, when acoustic wave reaches the ionosphere, it can induce a field-aligned current pulse and HF turbulence in the ionospheric E region. The presence of natural waveguides, such as the waveguide for atmospheric gravity waves, the atmospheric TN waveguide, the Alfvén and FMS waveguides, etc., results in modulation of a generated disturbance.

During the considered period, the magnetic storm represented the sum of two successive storms. The maximums of the main phases of the first and second storms were registered on November 8 ($Dst \sim -373$ nT) and November 10 ($Dst \sim -289$ nT), respectively (see Fig. 1 and the measurements of the magnetic field components at IZMIRAN Moscow magnetic observatory illustrated in Fig. 26). Precisely at that time, the most intense geomagnetic disturbances in the nightside sector of the magnetosphere were observed on the Earth's surface.

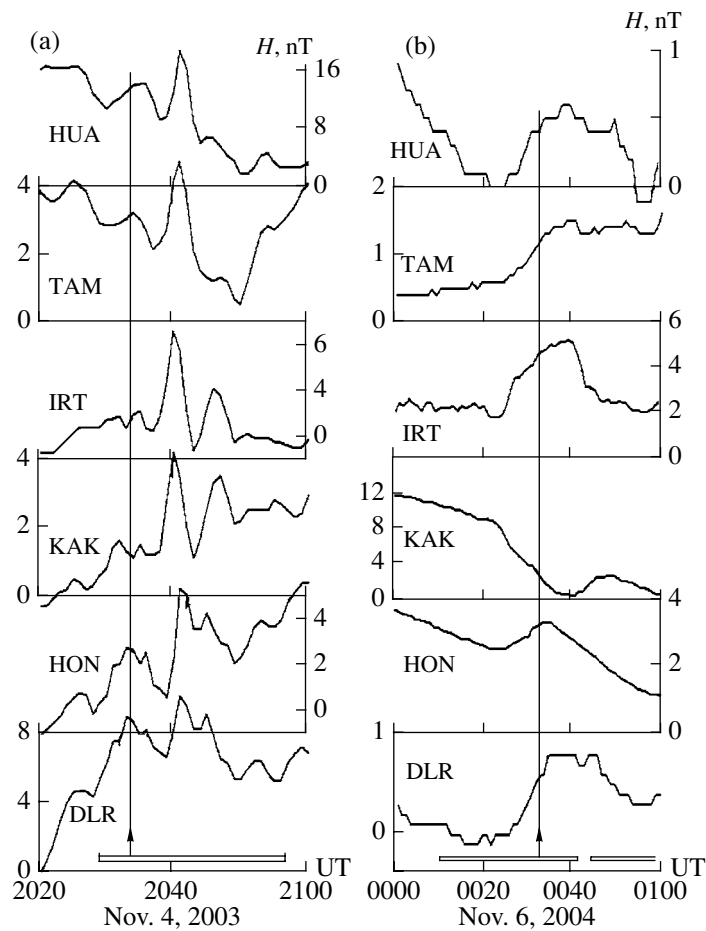


Fig. 25. Illustration of the global character of the geomagnetic response to gamma flares. Fragments of the magnetograms (H components) at the low-latitude observatories in different longitudinal sectors (HUA: magnetic latitude 21.03, MLT = UT - 5; TAM: 5.85, UT - 4; IRT: 47.10, UT + 7; KAK: 29.04, UT + 9; HON: 21.74, UT - 11; DLR: 38.92, UT - 7) for the events of (a) November 4, 2003, and (b) November 6, 2004. Rectangles and an arrow correspond to the gamma emission duration and time of maximum, respectively.

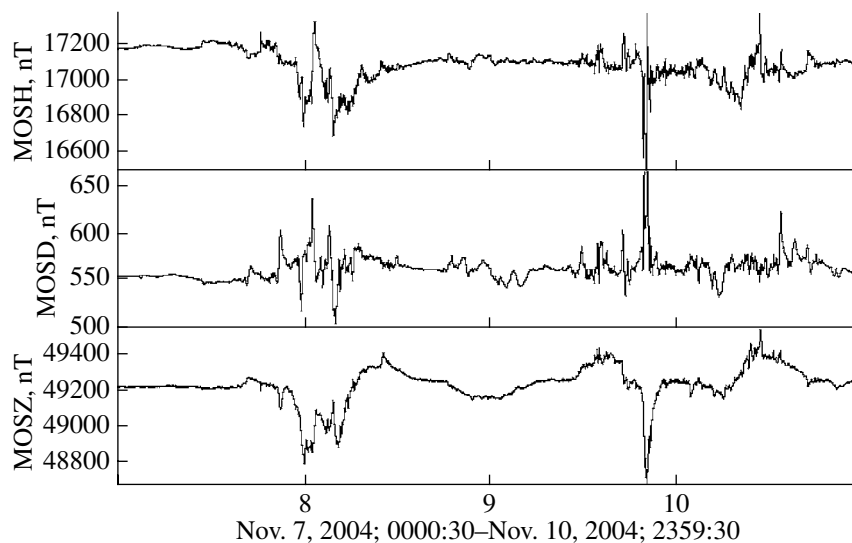


Fig. 26. Variations in the magnetic field components according to data of Moscow (IZMIRAN) magnetic observatory.

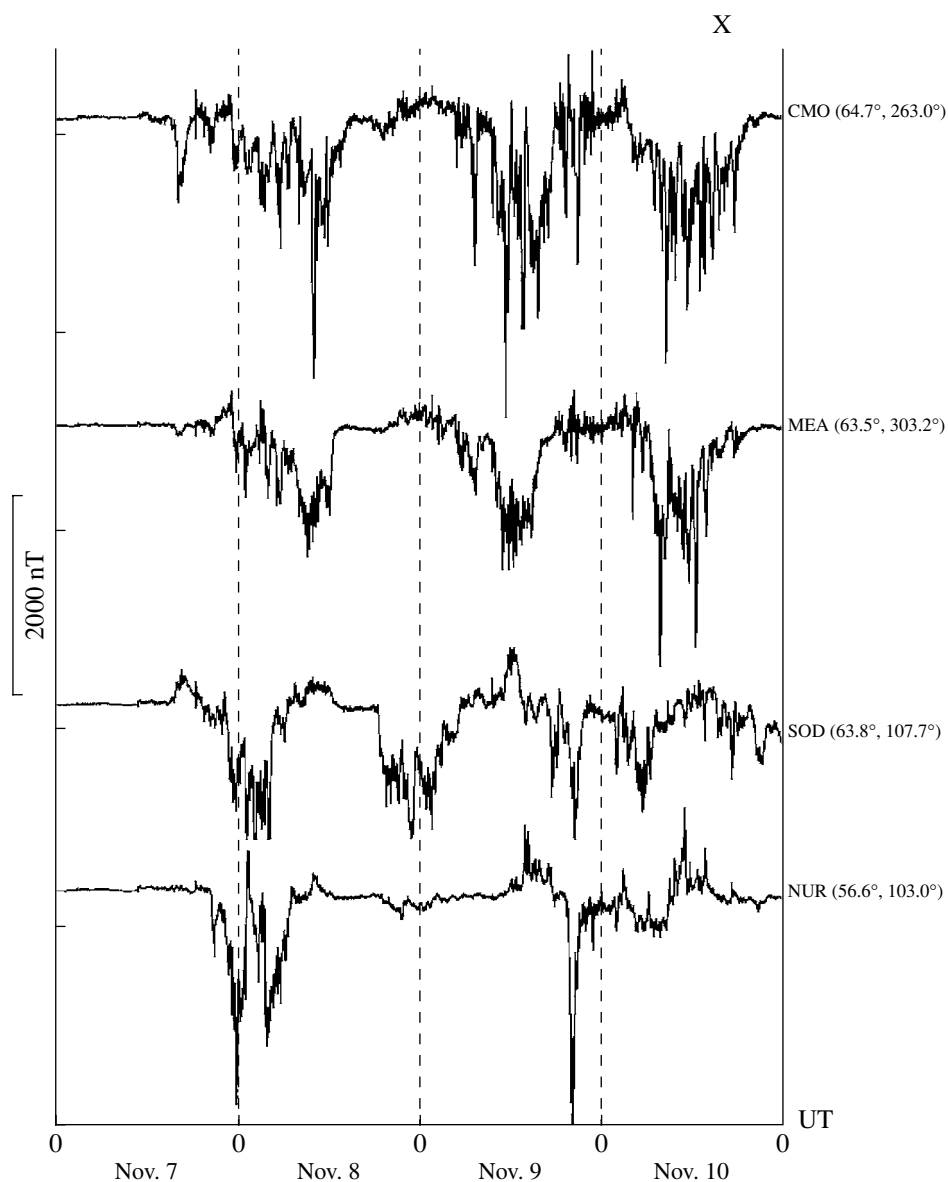


Fig. 27. Magnetograms from the observatories at antipodal points (for details see the text). Observatory codes and geomagnetic coordinates are shown on the right.

Figure 27 presents the magnetograms of the field X component for November 7–10, 2004, at four observatories located in the antipodal regions (i.e., in the regions separated by ~ 12 h in longitude). Geomagnetic midnight begins at 1100, 0830, 2130, and 2200 UT at College (CMO), Meanook (MEA), Sodankyla (SOD), and Nurmijarvi (NUR) observatories, respectively (i.e., in the nighttime and daytime at two first and last observatories, respectively). It is clear that the substorm amplitude in the nightside sector (CMO, MEA) reached 2000 nT on November 8 and 10. Prolonged disturbances had the form of isolated pulse bursts of duration 20–40 min and with an intensity of up to 400 nT.

It is interesting to note that the same and even more intense nighttime disturbances (especially at CMO)

were also registered on November 9, when the initial phase of the second superstorm developed against a background of the recovery phase of the first storm and the Dst values were about -100 nT. CMO and MEA are separated by only 1.2° in latitude but by 40° in longitude. The intensity of geomagnetic disturbances at these observatories differed several times, as in the nighttime during the main phase of the first superstorm of November 8, which indicates that the processes were largely local.

At the Scandinavian meridian (SOD, NUR), the maximal disturbances were also registered in the local nighttime. The most intense substorm (up to 3000 nT) was registered near midnight on November 9 at NUR. An interesting substorm was observed at night of

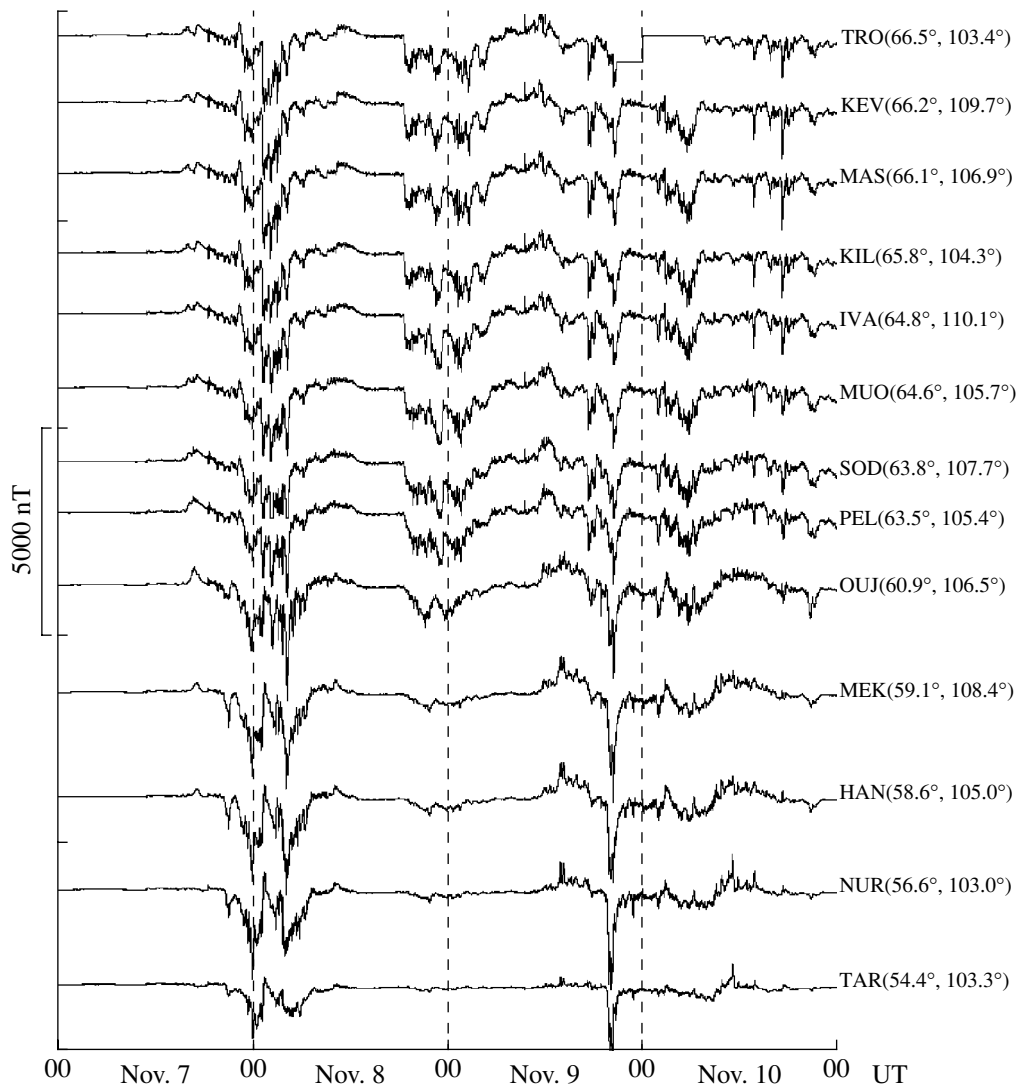


Fig. 28. Magnetograms from the Scandinavian observatories for November 7–10, 2004. Observatory codes and geomagnetic coordinates are shown on the right.

November 8–9 at SOD. This substorm was not observed at NUR lower-latitude observatory. In the dayside sector (CMO, MEA), Pc5 geomagnetic pulsations with the characteristics typical of resonance oscillations of the magnetosphere were observed at that time.

We now consider in more detail the latitudinal features of geomagnetic disturbances at the Scandinavian meridian (Fig. 28) at the dense IMAGE network of ground observatories. Two intense substorms with the maximal amplitude at latitudes lower than 60° were registered after local midnight on November 8 and were accompanied by riometer absorption bursts of up to 5–6 dB. At higher latitudes, the series of impulsive disturbances with an amplitude of up to 1500 nT was observed at that time.

Near midnight on November 9 (at 1700 UT), the substorm with a clearly defined main phase (no

observed at latitudes lower than 61°) originated at high geomagnetic latitudes (64° – 67°). Then new, much more intense (up to 3000 nT), substorm began at about 2000 UT and was observed in the wide range of latitudes. This substorm had the maximal intensity at latitudes of about 56° (NUR), where the electrojet center was located judging by the variations in the Z component on the profile of stations. The substorm was accompanied by the burst of riometer absorption the maximum of which (7 dB) was observed at 63° latitude, i.e., was higher in latitude than the current jet center.

On the night of November 8–9, intense (up to 1500 nT) impulsive disturbances (observed only at latitudes higher than 61° , below which the oscillation amplitude sharply decreased with decreasing latitude) were registered at the Scandinavian meridian (see above).

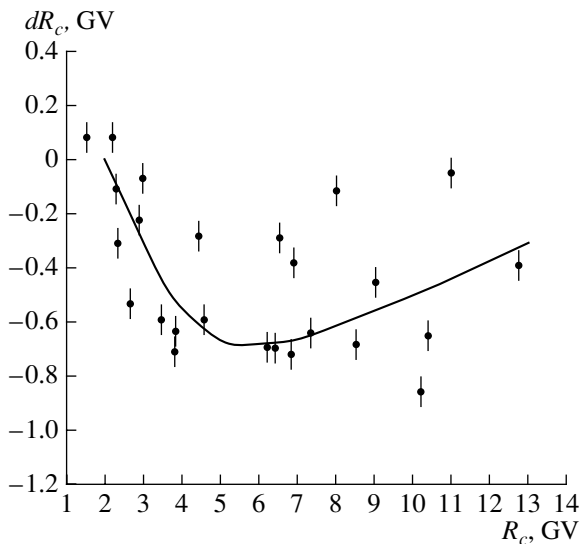


Fig. 29. Latitudinal distribution of the geomagnetic cutoff rigidity variations (dR_c) at the maximum of the magnetic storm of November 8, 2004.

Figure 28 indicates that all nights under discussion were characterized by a distinct change in the mode of magnetic disturbances at a geomagnetic latitude of about 60° . Hence, we can assume that this latitude corresponds to the polar boundary of the auroral zone. The nightside auroral zone also sharply shifted toward low latitudes during the superstorms of October 2003.

Judging by the Dst variations, the storm recovery phase began after 2100 UT on November 10. Very intense (up to 500 nT) quasimonochromatic Pc5 geomagnetic pulsations were generated during this phase of the superstorms observed in October and November 2003 [Kleimenova and Kozyreva, 2005]. However, such intense Pc5 pulsations were not observed during the recovery phase of the November 2004 superstorm. Only isolated bursts of oscillations with periods of about 4–5 min and with a maximal amplitude of 50–60 nT were registered in the dawnside–dayside sector at the Scandinavian meridian.

The described situation was also reflected in the GCR behavior in the form of the so-called magnetospheric effect of an increase in the CR intensity. According to the neutron monitor count rate (see Fig. 29), an increase in the CR intensity during the magnetic storm main phase was much larger at middle- and low-latitude stations than at high-latitude ones, which can actually be considered as the magnetospheric effect of CRs at these stations. The residual variance during counting performed according to the GSM method is considerable at that time, which indicates that the magnetospheric effect was not taken into account. Thus, the effects of interplanetary and geomagnetic origin most probably simultaneously manifested themselves during this event.

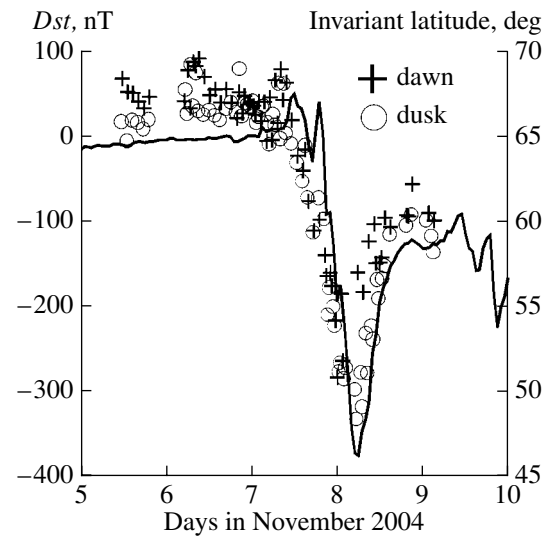


Fig. 30. Variations in the penetration boundaries of protons with energies of 1–5 MeV in the dawnside (crosses) and duskside (circles) sectors of the magnetosphere during the magnetic storm of November 8, 2004. The solid curve shows the Dst variation.

Changes in the geomagnetic cutoff rigidity during this effect were calculated for different stations using the method described in [Baisultanova *et al.*, 1995; Belov *et al.*, 2005a]. The distribution of the variations in these rigidities (dR_c) as compared to the rigidities during the quiet period in 2000 (factually, the latitudinal distribution) is shown in Fig. 29 for 0600–0700 UT on November 8 at a minimal value of the Dst variation for this effect. It is evident that the rigidity variations were maximal (about 0.7 GV) at latitudes corresponding to a geomagnetic cutoff rigidity of 5–6 GV, which confirms that the magnetosphere was less disturbed during this period than during the magnetic storm in November 2003 [Belov *et al.*, 2004b].

4.3. SCR Penetration Boundaries

As was mentioned previously, the transfer of active processes into the inner magnetosphere is one of the main features of a magnetic storm. In the near-Earth space, the SCR structure and fluxes depend on the geomagnetic field structure. As was done in [Panasyuk *et al.*, 2004] for the period of storms in October 2003, we use here the fluxes of low-energy SCR protons, registered during the CORONAS-F experiment, as a factor adequately reflecting transformations of the magnetospheric structure during a storm. Studying the dynamics of the boundaries of SCR penetration into the Earth's magnetosphere gives valuable information about a change in the geomagnetic field topology during geomagnetic disturbances. The dynamics of the boundary of solar proton and electron penetration is good indicator of the magnetospheric structure (see,

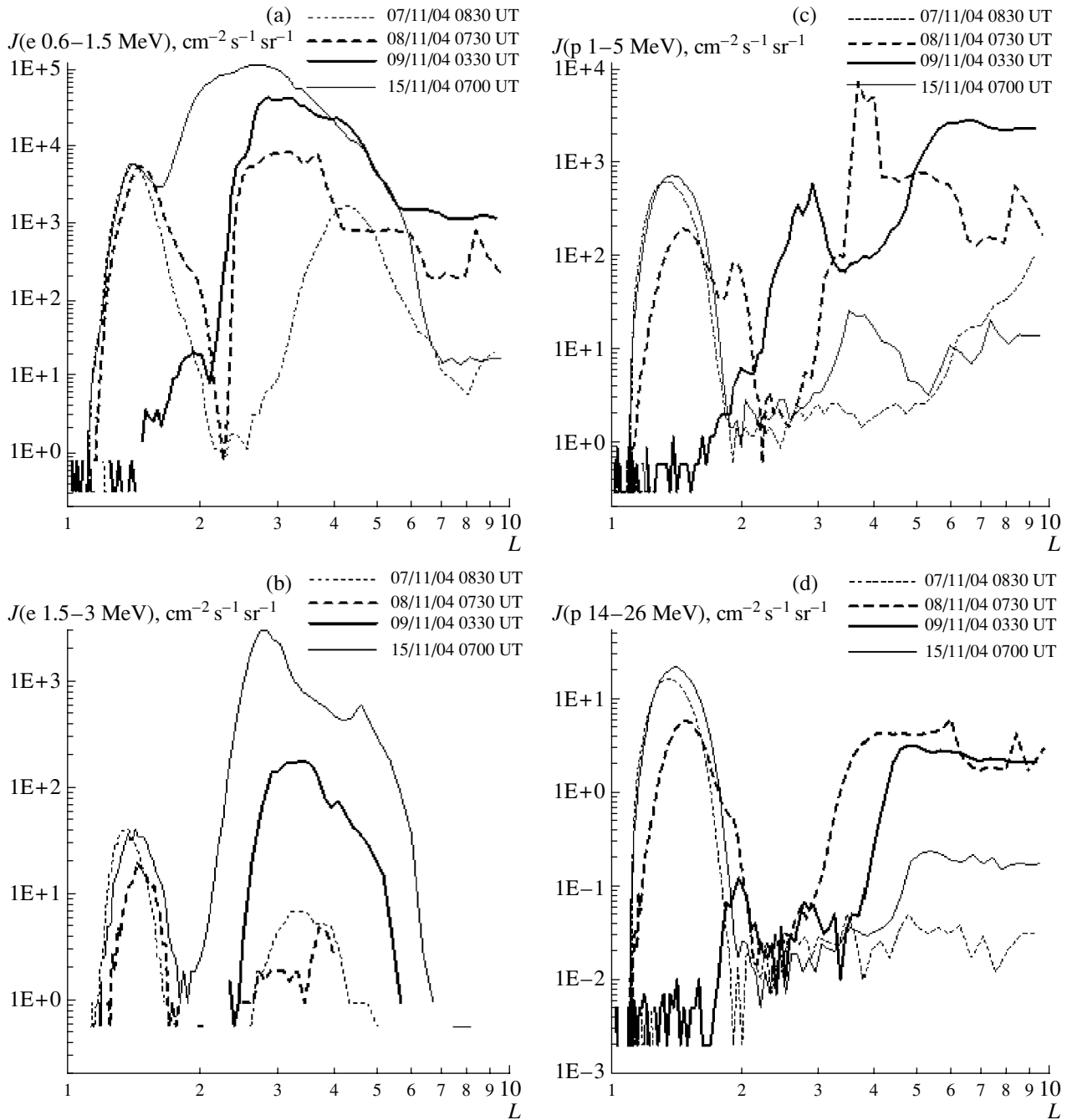


Fig. 31. Comparison of the profiles of the radiation belt particle fluxes: electrons with energies of (a) 600 keV–1.5 MeV and (b) 1.5–3 MeV; protons with energies of (c) 1–5 MeV and (d) 14–26 MeV.

e.g., [Darchieva *et al.*, 1990; Panasyuk *et al.*, 2004] and references therein).

SCRs with energies of 1–5 MeV have been registered in the polar caps since October 30, but we have studied the SCR penetration boundaries beginning from November 5, i.e., before the magnetic storm. As was mentioned, the CORONAS-F data are absent for November 10–15. Nevertheless, the available data

make it possible to trace the penetration boundary dynamics before the magnetic storm of November 8 and at the beginning of this storm. The flux of protons at the penetration boundary decreases rather gradually; therefore, different criteria can be used to analyze the position of this boundary. As was done in [Panasyuk *et al.*, 2004], we use the criterion traditional for the previous NIIYaF works: a factor of 2 decrease as compared to the maximum.

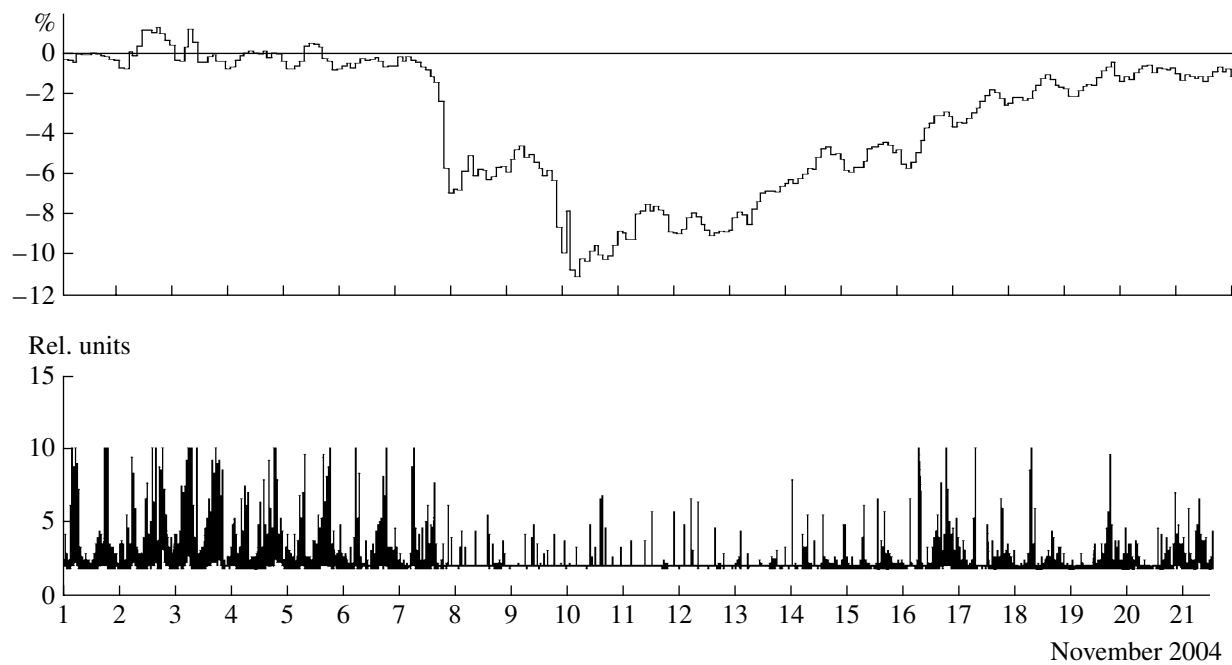


Fig. 32. Time variations in the neutron monitor data and magnetic component of atmospheric pulses in the frequency band 1–300 Hz in November 2004.

Figure 30 demonstrates the time variations in the penetration boundary of protons with energies of 1–5 MeV. It is clear that the prestorm boundary is located near 67° – 68° (i.e., near $L = 6$) both in the dawnside and duskside sectors (insignificant fluctuations are ignored). Figure 30 also indicates that the extreme low-latitude position of the boundaries in the dawnside and duskside sectors corresponds to the instants when the Dst variation amplitude was maximal during the storm of November 8. However, the values of the minimal invariant latitude are different for these sectors. The minimal invariant latitude of the boundary (Λ_b) is about 51° ($L = 2.5$) and 48° ($L = 2.3$) for the dawnside and duskside sectors, respectively. According to Fig. 30, the dynamics of the boundaries is in good agreement with the Dst variations during the main phase of this storm. As was assumed previously [Panasyuk *et al.*, 2004], a similar behavior of the boundaries in the dawnside and duskside sectors can be explained by the fact that particles are carried to drift orbits at the deepest penetration levels, as a result of which invariant longitudes on the day and night sides of the magnetosphere become equal.

4.4. Radiation Belt Variations

The dynamics of the Earth's radiation belts is one of the main physical processes during magnetic storms [Li and Temerin, 2001; Panasyuk *et al.*, 2004; Yermolaev *et al.*, 2005]. Let us trace the radiation belt dynamics during the strong magnetic storms at the beginning of November 2004 based on the CORONAS-F satellite

data. At that time, this satellite had the polar orbit with an inclination of 82.5° and a height of approximately 400 km. At such parameters of the orbit, the CORONAS-F instruments could register trapped radiation only in the region of the South Atlantic magnetic anomaly. Figures 31a–31d show the variations in the particle fluxes in the radiation belts (electrons with energies of 600 keV–1.5 MeV and 1.5–3 MeV; protons with energies of 1–5 and 14–26 MeV) in the morning sector of MLT. The L -shell nos. and particle flux intensities are plotted on the abscissa and ordinate, respectively. The data on the radiation belts on November 7 (thin dotted line) are used as an initial state of the belt before the magnetic storms: the maximum of the outer belt is located at $L = 4.5$; the slot between the belts, at $L = 2.5$. The data for October 8 (thick dotted line) and November 9 (thick solid line) were obtained almost immediately after the main phase and during the recovery phase of the first storm, respectively. Unfortunately, on that day the satellite crossed the inner belt only once at a large distance to the east of the Brazilian magnetic anomaly center; therefore, data on particle fluxes in the inner belt were not obtained on that day. Since information was absent during November 10–14, we could analyze the storm effect on the radiation belts only on November 15 (thin solid line), i.e., at the very end of the second storm recovery phase. Nevertheless, the data presented in Figs. 31a–31d contain important information about the radiation belt dynamics.

It is clear that, on November 8, the intensity of 1.5–3 MeV electrons at $L = 3$ – 3.5 pronouncedly decreased, the boundary of electrons with energies of 0.6–

1.5 MeV shifted toward the Earth to approximately $L = 2.2$, and the polar cap was filled with solar electrons of these energies. Figures 31c and 31d evidently demonstrate the proton penetration boundaries at $L = 3-3.5$ for energies of 14–26 and 1–5 MeV, respectively. On November 9 the outer belt became pronouncedly wider (this is evident for both electron energy channels); the intensity of electrons with energies of 600 keV–1.5 MeV and 1.5–3 MeV increased by more than one and by one and a half orders of magnitude, respectively; and the outer belt maximum shifted toward the Earth. It is clear that the observed dynamics of electron fluxes in the outer belt is very similar to the changes in the Earth's outer radiation belt during the storms of October–November 2003 [Panasyuk *et al.*, 2004; Yermolaev *et al.*, 2005]. The absence of significant fluxes of 1–5 MeV protons in the inner belt is related exclusively to the geographic position of the only satellite orbit in the spatial region. The protons with energies of 1–5 MeV had the additional maximum at $L = 2.8-3$, which is also similar to the data obtained in 2003 [Panasyuk *et al.*, 2004; Yermolaev *et al.*, 2005]. Five days later (on November 15) the electron outer belt continued widening, the fluxes of electrons (especially with energies of 1.5–3 MeV) in the outer belt increased as before, and the outer belt maximum shifted to $L = 2.3-2.5$. At that time the peak of 1–5 MeV protons shifted to $L = 3.8$, and the flux of protons with energies of 14–26 MeV in the polar caps was still higher than the background value obtained on November 7 by almost an order of magnitude.

The presented data indicate that the radiation belt dynamics during the November 2004 storms was rather similar to such a dynamics during the strong storms of October–November 2003 described in [Panasyuk *et al.*, 2004; Yermolaev *et al.*, 2005], namely:

- (i) the intensity of the flux of 1.5–3 MeV electrons decreased during the magnetic storm main phase;
- (ii) during the recovery phase the intensity of the electron fluxes from the Earth's outer radiation belt pronouncedly increased, the electron belt widened, and the belt maximum shifted to smaller L ;
- (iii) the additional maximum of protons with energies of 1–5 MeV appeared near $L = 3$.

4.5. Atmospheric Electric Field in the ELF Band

According to recent concepts (see, e.g., [Ermakov *et al.*, 2003]), CRs are one of the main sources of atmospheric ionization, especially at high latitudes where the intensity of another ionizing factor—thunderstorm activity—is much lower than at low latitudes. In this case only part of low-latitude lightning discharges has so powerful electromagnetic pulses that can reach high-latitude regions and pronouncedly exceed the local fluctuation electromagnetic background. The main energy of similar pulses at an observation point varies

from several hertz to several tens of kilohertz (see, e.g., [Remizov, 1985]).

When analyzing atmospherics registered in Yakutsk at frequencies of 0.3–10 kHz, Mullayarov *et al.* [2003] concluded that Forbush decreases in GCR intensity lead to an increase in thunderstorm activity and in the number of atmospherics. However, the plots presented by these researchers indicate that, in our opinion, the intensity of atmospherics only recovers, rather than increases, during the Forbush effect after a decrease in the intensity caused by an increase in relativistic solar protons. As is known, protons precipitate into the Earth's atmosphere before Forbush decreases and result in the formation of a thick ionization layer in the lower ionosphere, which hinders propagation of atmospherics, especially at high latitudes.

It is known that the amplitude spectra of atmospheric electromagnetic pulses have two maximums at distances larger than several thousand kilometers, namely: 2–10 kHz and several kilohertz—several hundreds of kilohertz.

From July 2003, atmospheric electromagnetic pulses at frequencies of 1–300 Hz have been continuously observed at the Apatity atmospheric station, Polar Geophysical Institute (67°33' N, 33°20' E) [Roldugin *et al.*, 2003]. According to the data of the Apatity neutron supermonitor, considerable Forbush decreases (decreases in GCR intensity by 4% and more) were registered five times during the period of observations from July 2003 to November 2004. A decrease in the magnetic components of atmospheric pulses corresponded to a Forbush decrease in GCRs in all cases.

Figure 32 illustrates the observations performed in Apatity in November 2004: the supermonitor data (upper plot) and the behavior of the magnetic component of atmospheric pulses in the ELF band, 1–300 Hz (lower plot).

To all appearance, atmospheric electromagnetic pulses in the band 1–300 Hz considered in the present work are mainly caused by lightning strokes between a cloud and the upper atmosphere, i.e., sprites and jets (see, e.g., [Morozov, 2002] and a summary therein). A Forbush decrease in GCR intensity leads to a decrease in the degree of ionization of the upper atmospheric layers and, as a consequence, to a decrease in the intensity of formation of sprites and jets, which in turn results in a decrease in ELF signals.

4.6. Electrotelluric Field Response

Variations in the electrotelluric field and their relations to other heliogeophysical phenomena were studied at the Karymshina complex observation (CO), Kamchatka branch, Geophysical Service, Russian Academy of Sciences, which is located in the southern part of the Kamchatka Peninsula at a distance of approximately 30 km from the Pacific coast (52.8° N, 158.15° E). CO is located at a considerable distance

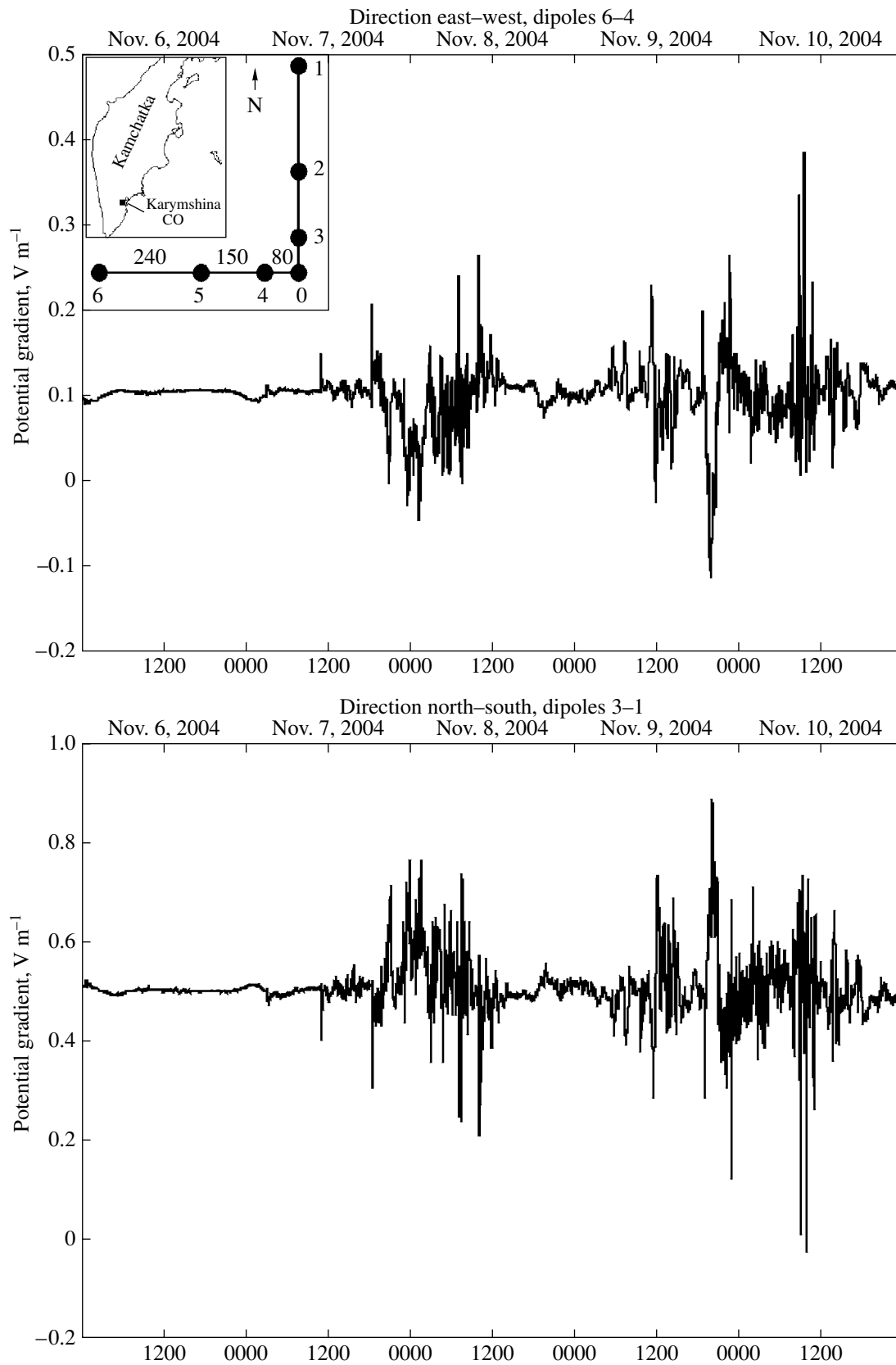


Fig. 33. ETP registered by six mutually perpendicular dipoles during the magnetic storms of November 7–10, 2004. Minute averaging of gradients. Inset shows the position of electrodes in the system of ETP registration at Karymshina CO. Distances between electrodes are given in meters.

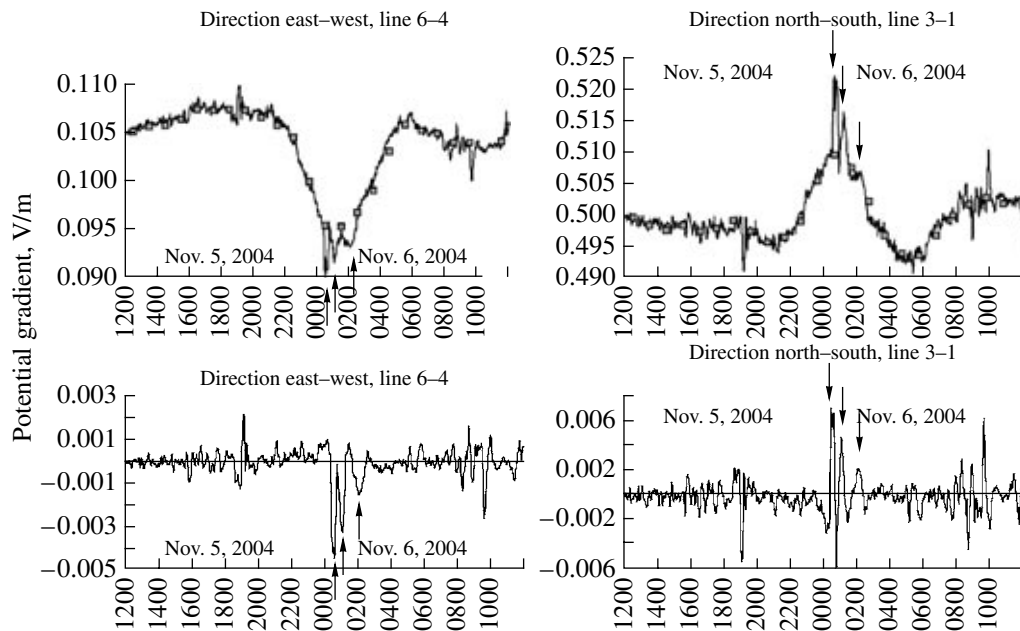


Fig. 34. ETP registered by six mutually perpendicular dipoles during the solar flares at 0011–0248 UT on November 6, 2004. Minute averaging of ETP gradients. Three peaks corresponding to three X-ray flares are registered on the upper plots against a background of the solar-diurnal variation. (Hourly values of the solar diurnal variation are marked by dots.) The lower plots show the ETP variations during the same period with a filtered-out solar-diurnal variation.

from possible sources of anthropogenic noise, which makes it possible to realize the maximal sensitivity of recording equipment.

At Karymshina CO, the electrotelluric potential (ETP) is registered by six dipoles, which belong to two systems of north–south ($\varphi_1, \varphi_2, \varphi_3$) and west–east ($\varphi_4, \varphi_5, \varphi_6$) lines (see the inset in Fig. 33). The registration range is ± 2 V, readings are taken at an interval of 1 Hz, the threshold sensitivity of a geovoltmeter is ~ 30 μ V, and the dynamic range of registered signals is not less than 102 dB. The potential is counted off relative to detector marked by 0 on the scheme, for which the potential value is taken equal to zero.

The Karymshina CO records of solar flares (S_{FE} magnetic disturbances) and of numerous magnetic storms illustrate the ETP response to magnetospheric and ionospheric disturbances caused by solar activity. Figures 33 and 34 show the records of two magnetic storms that occurred on November 7–10, 2004, and of the flare event observed on November 6, 2004, respectively. The latter event occurred near local noon during the period of weakly disturbed geomagnetic conditions. This is apparently the only record of the flare in the Kamchatka geoelectric field on the Russian territory.

During magnetic storms, magnetic variations induce electric fields in any conducting medium. Since the upper layers of the Earth’s crust are electrically conductive, currents are induced here. Magnetic storms are clearly defined in ETP records almost in all cases.

ETP disturbances during solar flares, as well as their effect on the S_{FE} geomagnetic field, are shown in

records as a burst or an impulsive change lasting several tens of minutes. In the geoelectric and geomagnetic fields, the flare effect can be observed only under quiet geomagnetic conditions near local noon. The HF electromagnetic emission of a solar flare increases ionospheric conductivity and temporarily changes normal ionospheric S_q currents on the sunward side of the Earth, parametrically affecting the current in the global electrical network, which in turn influences electric processes in the upper part of the Earth’s crust. The ETP response to a solar flare is of a complex origin and is related to the induction effect and to a temporary change in the conductivity of the global electric circuit during a solar flare.

5. CONCLUSIONS

As follows from the observations performed for the last several years, the main surprises took place during the phase of decline of the current solar cycle (cycle 23). Solar activity was high in 2001–2003, although the solar maximum (at least with respect to the number of sunspots) was observed in 2000. For example, the events of October–November 2003 are extreme with respect to a number of parameters [Veselovsky *et al.*, 2004; Panasyuk *et al.*, 2004; Yermolaev *et al.*, 2005]. In this paper, we presented the experimental observations of the Sun, heliosphere, and magnetosphere and performed a preliminary analysis for the next period of high disturbance, which was accompanied by the strongest geomagnetic storm of November 8–10, 2004, with $Dst = -373$ nT. This work not only presents comprehen-

sive and various experimental data of observations in different regions but also demonstrates possible cause–effect relations between different phenomena in the complex chain of solar–terrestrial physics.

ACKNOWLEDGMENTS

We are grateful to the teams operating the SOHO/LASCO coronagraph; SOHO/EIT telescope; CORONAS-F, GOES, and ACE satellites; Big Bear and Medon observatories; and the series of ground-based stations for data used in the present work. The CME difference images were obtained based on the IDL program developed by V. V. Grechnev (ISZF, Irkutsk).

This work was supported by the Russian Foundation for Basic Research (project nos. 03-02-16049, 03-51-6206, 04-02-16131, 04-02-16152, 04-02-17332, and 05-02-16228); Ministry of Education and Science of the Russian Federation (grant NSh 1445.2003.2); “Universities of Russia” (project UR.02.02.509/05-1); INTAS (project 03-51-3738); OFN RAN programs “Plasma Processes in the Solar System” and “Physics of the Atmosphere: Electric Processes and Radar Methods of Studies”; RAN program “Solar Activity and Physical Processes on the Sun–Earth System”; and Slovak VEGA grant agency (project no. 4064).

REFERENCES

1. S.-I. Akasofu, N. Olmsted, E. J. Smith, *et al.*, “Solar Wind Variations and Geomagnetic Storms: A Study of Individual Storms Based on High Time Resolution ISEE-3 Data,” *J. Geophys. Res.* **90**, 325 (1985).
2. L. Baisultanova, A. Belov, and V. Yanke, “Magnetospheric Effect of Cosmic Rays within the Different Phases of Magnetic Storms,” in *Proceedings of the 24th ICRC, 1995*, Vol. 4, pp. 1090–1094.
3. I. L. Beigman, S. A. Bozhenkov, I. A. Zhitnik, *et al.*, “Solar EUV Spectra Obtained during the SPIRIT Experiment on the CORONAS-F Spacecraft. I. Catalog of Lines in the 280–330 Å Band,” *Pis'ma Astron. Zh.* **31** (1), 39–58 (2005).
4. A. V. Belov, L. M. Baisultanova, E. A. Eroshenko, *et al.*, “Unusually Great Magnetospheric Effect in Cosmic Rays on November 20, 2003,” *Izv. Akad. Nauk, Ser. Fiz.* **69** (6), 857–860 (2005a).
5. A. V. Belov, E. A. Eroshenko, and V. G. Yanke, “Events of October–November 2003 in Ground-Based Observations of Cosmic Rays,” *Geomagn. Aeron.* **45** (1), 51–57 (2005b) [*Geomagn. Aeron.* **45**, 47–53 (2005b)].
6. A. V. Belov, E. A. Eroshenko, V. A. Oleneva, *et al.*, “What Determines the Magnitude of Forbush Decreases?,” *Adv. Space Res.* **27** (3), 625–630 (2001).
7. A. V. Belov, K. G. Gaidash, S. P. Ivanov, and Kh. D. Kanonidi, “Unusually High Geomagnetic Activity in 2003,” *Kosm. Issled.* **42** (6), 563–573 (2004).
8. J. Bendat and G. Piersol, *Random Data: Analysis and Measurement Procedures* (New York, 1986; Mir, Moscow, 1989).
9. V. M. Bogod, G. A. Gelfreikh, F. Ch. Drago, *et al.*, *astro-ph/0309444*.
10. V. M. Bogod and S. Kh. Tokhchukova, “Peculiarities of the Microwave Emission from Active Regions Generating Intense Solar Flares,” *Astron. Lett.* **29**, 263–273 (2003).
11. V. Bothmer, I. S. Veselovsky, A. V. Dmitriev, *et al.*, “Solar and Heliospheric Reasons for Geomagnetic Perturbations during the Growth Phase of the Solar Cycle 23,” *Sol. Syst. Res.* **36**, 498–505 (2002).
12. H. V. Cane and I. G. Richardson, “Interplanetary Coronal Mass Ejections in the Near-Earth Solar Wind during 1996–2002,” *J. Geophys. Res.* **108A**, SSH 6 (2003).
13. H. V. Cane, R. E. McGuire, and O. O. Von Rosenvince, “Two Classes of Solar Energetic Particle Events Associated with Impulsive and Long-Duration Soft X-Ray Flares,” *Astrophys. J.* **301**, 449 (1986).
14. I. V. Chashei and V. I. Shishov, “On the Effect of Turbulence on the Interplanetary Shock Propagation,” *Pis'ma Astron. Zh.* **21**, 716–720 (1995).
15. I. M. Chertok, “Large-Scale Activity during Powerful Solar Eruptive Events of November 2004 according to the SOHO/EIT UV Telescope Data,” *Astron. Zh.*, **81** (5), 447–458 (2005).
16. I. M. Chertok, V. A. Slemzin, S. V. Kuzin, *et al.*, “Solar Eruptive Event of November 4, 2001, according to Data of the SPIRIT telescope on the CORONAS-F Satellite,” *Astron. Zh.* **81** (5), 447–58 (2004).
17. D. G. Cole, “Space Weather: Its Effects and Predictability,” *Space Sci. Rev.* **107** (1–2), 295–302 (2003).
18. N. U. Crooker, “Solar and Heliospheric Geoeffective Disturbances,” *J. Atmos. Sol.–Terr. Phys.* **62**, 1071 (2000).
19. I. A. Dagnis, J. U. Kozyra, Y. Kamide, *et al.*, “Intense Space Storms: Critical Issues and Open Disputes,” *J. Geophys. Res.* **108A**, SMP 17 (2003).
20. A. Dal Lago, L. E. A. Viera, E. Echer, *et al.*, “Comparison between Halo CME Expansion Speeds Observed on the Sun, the Related Shock Transit Speeds to Earth and Corresponding Ejecta Speeds at 1 AU,” *Sol. Phys.* **222**, 328 (2004).
21. L. A. Darchieva, T. A. Ivanova, E. N. Sosnovets, and L. V. Tverskaya, “Dynamics of Equatorial and Polar Boundaries of Penetration of Solar Protons with Energy >1 MeV into the Magnetosphere during the Strong Magnetic Storm,” *Geomagn. Aeron.* **30** (5), 856–858 (1990).
22. A. V. Dmitriev, N. A. Crosby, and J.-K. Chao, “Interplanetary Sources of Space Weather Disturbances in 1997 to 2000,” *Space Weather* **3**, S03001 (2005).
23. M. Dryer, “Interplanetary Shock Waves Generated by Solar Flares,” *Space Sci. Rev.* **15**, 403–437 (1974).
24. E. Echer and W. D. Gonzalez, “Geoeffectiveness of Interplanetary Shocks, Magnetic Clouds, Sector Boundary Crossings and Their Combined Occurrence,” *Geophys. Res. Lett.* **31** (9), L09808 (2004).
25. V. T. Ermakov, Yu. I. Stozhkov, and N. S. Svirzhevskii, “Main Atmospheric Ionization Sources,” in *Proceedings of the 5th Russian Conference on Atmospheric Electricity, Vladimir, 2003* (Vladimir Gos. Univ., Vladimir, 2003), Vol. 1, pp. 63–65.

26. M. V. Eselevich and V. G. Eselevich, "Sporadic Plasma Flows and Their Sources during Extreme Solar Activity from October 26 to November 6, 2003," *Kosm. Issled.* **42** (6), 1–13 (2004).
27. V. G. Eselevich and V. G. Fainshtein, "An Investigation of the Relationship between the Magnetic Storm *Dst*-Index and Different Types of Solar Wind Streams," *Ann. Geophys.* **11**, 678 (1993).
28. W. D. Gonzalez, A. Dal Lago, A. L. Clua De Gonzalez, *et al.*, "Prediction of Peak-*Dst* from Halo CME/Magnetic Cloud-Speed Observations," *J. Atmos. Sol.–Terr. Phys.* **66**, 161–165 (2004).
29. W. D. Gonzalez, A. O. Tsurutani, and A. L. Clua De Gonzalez, "Interplanetary Origin of Geomagnetic Storms," *Space Sci. Rev.* **88**, 529 (1999).
30. R. R. Kane, "How Good is the Relationship of Solar and Interplanetary Plasma Parameters with Geomagnetic Storms?," *J. Geophys. Res.* **110A** (2005) (in press).
31. N. G. Kleimenova and O. V. Kozyreva, "Spatial–Temporal Dynamics of Pi3 and Pc5 Geomagnetic Pulsations during the Extreme Magnetic Storms in October 2003," *Geomagn. Aeron.* **45** (1), 71 (2005) [*Geomagn. Aeron.* **45**, 71–79 (2005)].
32. V. I. Kozlov and N. N. Tugolukov, "Cosmic Ray Intensity Scintillation," *Geomagn. Aeron.* **32** (3), 153–159 (1992).
33. S. V. Kuzin, I. A. Zhitnik, S. A. Bozhenkov, *et al.*, "Diagnostic of Solar Corona Plasma by Means of EUV Spectroheliograph RES-C on CORONAS-F Spacecraft," *Adv. Space Res.* (2005) (in press).
34. S. N. Kuznetsov, A. V. Bogomolov, Yu. P. Gordeev, *et al.*, "Preliminary Results of the Experiment Performed Using the CORONAS-I SCR Equipment," *Izv. Akad. Nauk, Ser. Fiz.* **59**, 2–6 (1995).
35. S. N. Kuznetsov, K. Kudela, S. P. Ryumin, and Y. V. Gotselyuk, "CORONAS-F Satellite - Tasks for Study of Particle Acceleration," *Adv. Space Res.* **30**, 1857–1863 (2002).
36. X. Li and M. A. Temerin, "The Electron Radiation Belt," *Space Sci. Rev.* **95**, 569–580 (2001).
37. W. Lyatsky and A. Tan, "Solar Wind Disturbances Responsible for Geomagnetic Storms," *J. Geophys. Res.* **108A**, SMP 21 (2003).
38. Y. P. Maltsev, "Points of Controversy in the Study of Magnetic Storms," *Space Sci. Rev.* **110** (3-4), 227–277 (2004).
39. A. Mitra, *Ionospheric Effects of Solar Flares* (Reidel, Boston, 1974; Mir, Moscow, 1977).
40. A. V. Moldavanov, "Stratospheric Discharges during Solar Gamma Flares," *J. Phys. D: Appl. Phys.* **36**, L1–L4 (2003).
41. V. N. Morozov, "Calculation of Thundercloud Electric Fields for Initiating Electric Discharges between Clouds and the Upper Atmosphere," *Geomagn. Aeron.* **42** (1), 121–129 (2002) [*Geomagn. Aeron.* **42**, 114–122 (2002)].
42. O. Motoba, O. Kikuchi, H. Luhr, *et al.*, "Global Pc5 Caused DP2-Type Ionospheric Current System," *J. Geophys. Res.* **107A**, SMP 7 (2002).
43. V. A. Mullayarov, V. I. Kozlov, *et al.*, "Manifestation of CR Variations in Thunderstorm Activity," in *Proceedings of the 5th Russian Conference on Atmospheric Electricity, Vladimir, 2003* (Vladimir Gos. Univ., Vladimir, 2003), Vol. 1, pp. 60–62.
44. V. N. Oraevskii, I. I. Sobel'man, I. A. Zhitnik, and V. D. Kuznetsov, "Complex Studies of Solar Activity on the CORONAS-F Satellite: New Results," *Usp. Fiz. Nauk.* **172** (8), 949–959 (2002).
45. M. I. Panasyuk, S. K. Kuznetsov, L. L. Lazutin, *et al.*, "Magnetic Storms in October 2003," *Kosm. Issled.* **42** (5), 509–554 (2004).
46. E. N. Parker, "Sudden Expansion of the Corona Following a Large Solar Flare and the Attendant Magnetic Field and Cosmic-Ray Effects," *Ap. J.* **133**, 1014–1025 (1961).
47. V. A. Parkhomov, "Geomagnetic Pulsations Related to Solar Flare Gamma Emissions," *Geomagn. Aeron.* **32**, 130 (1992).
48. M. I. Pudovkin, S. A. Zaitseva, and I. P. Oliferenko, "Magnetic Field of a Flare Flux," *Izv. Akad. Nauk SSSR, Ser. Fiz.* **41** (2), 242–251 (1977).
49. L. T. Remizov, *Natural Radio Noise* (Nauka, Moscow, 1985) [in Russian].
50. I. G. Richardson, E. W. Cliver, and H. V. Cane, "Sources of Geomagnetic Storms for Solar Minimum and Maximum Conditions during 1972–2000," *Geophys. Res. Lett.* **28**, 2569 (2001).
51. V. K. Roldugin, M. I. Beloglazov, *et al.*, "On Atmospheric Electricity Observations on the Kola Peninsula," in *Proceedings of the 5th Russian Conference on Atmospheric Electricity, Vladimir, 2003* (Vladimir Gos. Univ., Vladimir, 2003), Vol. 1, pp. 130–133.
52. R. Schwenn, A. Dal Lago, E. Huttunen, and W. D. Gonzalez, "The Association of Coronal Mass Ejections with Their Effects near the Earth," *Ann. Geophys.* **23**, 1033–1059 (2005).
53. N. R. Sheeley, Jr., R. A. Howard, M. J. Koomen, *et al.*, "Doppler Scintillation Observations of Interplanetary Shocks within 0.3 AU," *J. Geophys. Res.* **90**, 154 (1985a).
54. N. R. Sheeley, Jr., R. A. Howard, M. J. Koomen, and D. J. Michels, "Coronal Mass Ejection and Interplanetary Shock," *J. Geophys. Res.* **90**, 163 (1985b).
55. S. Kh. Tokhchukova and V. M. Bogod, "Detection of the Long-Term Microwave 'Darkening' before the 14 July 2000 Flare," *Sol. Phys.* **212**, 99–109 (2003).
56. B. T. Tsurutani, W. D. Gonzalez, F. Tang, and Y. T. Lee, "Great Magnetic Storm," *J. Geophys. Res.* **93**, 8519 (1988).
57. N. N. Tugolukov and V. I. Kozlov, "Relation between Cosmic Ray Intensity Scintillation and Solar Wind Parameters," *Geomagn. Aeron.* **31** (4), 715–716 (1991).
58. I. S. Veselovsky, V. Bothmer, A. V. Dmitriev, *et al.*, "Transequatorial Coronal Mass Ejection and the Related Powerful Geoeffective Disturbance in November 2004," *Astron. Vestn.* (2005) (in press).
59. I. S. Veselovsky, M. I. Panasyuk, S. I. Avdyushin, *et al.*, "Solar and Heliospheric Events in October–November 2003: Causes and Consequences," *Kosm. Issled.* **42** (5), 453–508 (2004).
60. I. S. Veselovsky, V. Bothmer, P. Cargill, *et al.*, "Magnetic Storm Cessation during Sustained Northward IMF," *Adv. Space Res.* (2005).

61. V. I. Vlasov, "Interplanetary Shock Velocity according to Radio-Astronomical Data," *Geomagn. Aeron.* **28**, 1–8 (1988).
62. D. J. Williams, J. F. Arens, and L. J. Lanzerotti, "Observations of Trapped Electrons at Low and High Altitudes," *J. Geophys. Res.* **73**, 5673–5696 (1968).
63. Chin-Chun Wu and R. P. Lepping, "Effect of Solar Wind Velocity on Magnetic Cloud-Associated Magnetic Storm Intensity," *J. Geophys. Res.* **107A**, SSH 3 (2002).
64. Yu. I. Yermolaev, M. Yu. Yermolaev, G. N. Zastenker, *et al.*, "Statistical Studies of Geomagnetic Storm Dependencies on Solar and Interplanetary Events: A Review," *Planet. Space Sci.* **53**, 189–196 (2005).
65. Yu. I. Yermolaev and M. Yu. Yermolaev, "On Certain Statistical Interrelations of Solar, Interplanetary, and Geomagnetic Disturbances during 1976–2000. 3," *Kosm. Issled.* **41** (6), 539 (2003).
66. Yu. I. Yermolaev, L. M. Zelenyi, G. N. Zastenker, *et al.*, "Solar and Heliospheric Disturbances that Resulted in the Strong Magnetic Storm of November 20, 2003," *Geomagn. Aeron.* **45** (1), 23–50 (2005) [*Geomagn. Aeron.* **45**, 20–46 (2005)].
67. V. Yurchyshyn, <http://sprg.ssl.berkeley.edu/RHESSI/rst/abstracts/yurchyshyn.txt>.
68. A. N. Zhukov, R. Van der Linden, P. Vanlommel, *et al.*, <http://www.congrex.nl/04c27>.
69. E. Ya. Zlotnik, "About Prevalence of Ordinary Wave in Microwave Emission of Solar Active Regions," *Radiophys. Quantum Electron.* **44**, 53–61 (2001).